MATERIALS, TECHNOLOGIES, CONSTRUCTIONS

"Special purpose technologies"

Redakcja naukowa:
dr Andrzej Chmielowiec

Stalowa Wola 2019

Table of Contents

Chapter 1.

Zenon OPIEKUN[1]
Bogdan KUPIEC[1*]
Magdalena LENIK[1]

TECHNOLOGICAL PROCESS OF WELDING ARMOX 500T ARMOUR STEEL PLATES

Abstract
The paper presents the course of the technological process of welding Armox 500T armour steel plates with the use of GMAW method with pulsating arc in the shield of gas ($98\%Ar + 2\%O_2$) with the use of filler metal in the form of wire designated as OK Autorod 16.95. Welded butt and corner joints of metal plates were made as butt welds and fillet welds with the use of appropriate experimentally determined welding parameters. On the grounds of visual metallographic examination and hardness measurements of joints made that way it has been found that the welded joints were of good quality, free of cracks, and their hardness in the heat affected zone (HAZ) was on the level of 440HV10.
Keywords:
Armox 500T steel, welding, structure of welded joints, GMAW method.

1. Introduction

Armour steel plates should guarantee effective protection against armour-piercing projectiles striking at high velocity [1–6]. For this reason, metal plates used for ballistic shields should be characterised with very good mechanical properties, especially with very high hardness and high retained plasticity of steel. Moreover, in view of the fact that bodies of armoured vehicles such as turrets of self-propelled howitzers or armoured troop-carriers are fabricated as welded structures, armour steel plates should show good susceptibility to welding (weldability). The steel with designation Armox 500T is an example of such material [7]. Obtaining good-quality Armox 500T armour steel plates meeting relevant requirements concerning their service properties is possible by subjecting them to appropriate heat treatment consisting in thermal hardening (quenching and low-temperature tempering). The basic chemical composition of

---

[1] Department of Casting and Welding, Rzeszow University of Technology,
 al. Powstańców W-wy 12, 35-959 Rzeszow, Poland
*kupiec@prz.edu.pl

the steel is as follows: 0.30%C; 0.30%Si; 1.2%Mn; 1.0%Cr; 1.8%Ni; 0.7%Mo; and 0.003%B. The steel is expected to contain little impurities, sulphur, and phosphorus, on the level of about 0.01% at the most. Chromium, molybdenum, manganese, and boron increase hardenability of the steel, and its specific chemical composition corresponds to the isothermal transformation (TTT) diagram with separated diffusion and bainitic-martensitic phase transitions [8].

The objective of the present paper is to present a technological process of welding thick (8 mm and 17 mm) plates of Armox500T steel. The welding parameters such as the welding speed, current intensity, arc voltage, plate bevelling , number of runs, and other factors chosen experimentally and developed as part of the present study, as well as the used filler metal enabled to make welded joints on the plates which are characterised with good service properties.

2. Materials and research methodology

The material used for the present study were Armox 500T steel plates with dimensions 150 mm × 150 mm and thickness of 8 mm and 17 mm, hardened thermally by quenching from temperature of about 860°C / 1 hour / oil and tempering at 180°C / 4 hours / air. Hardness of the steel after such thermal treatment was about 400HV10 on average. Chemical composition of the steel used in the welding tests is summarised in Table 1.1, whereas its microstructure after thermal hardening is presented in Figure 1.1.

Table 1.1. Chemical composition of Armox500T steel plates used in the study, % mas.

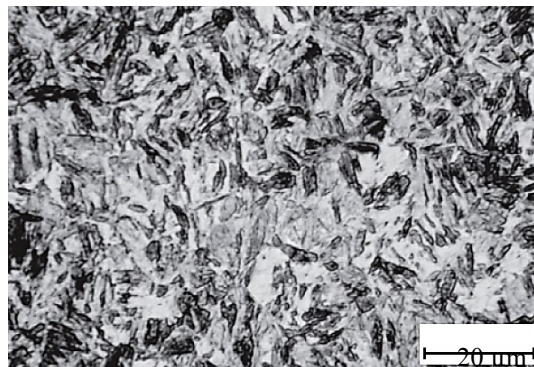| Steel designation	C	Si	Mn	P max.	S max.	Cr	Ni	Mo	B	CEV
Armox 500 T	0.30	0.30	1.2	0.010	0.010	1.0	1.8	0.7	0.003	0.75

Fig. 1.1. Microstructure of Armox500T steel after thermal hardening. Fine grains of tempered martensite. The section was etched with Kalling's reagent [1]

Welding of Armox500T steel plates was carried out with the use of MAG method in atmosphere of shielding gas containing 98%Ar + 2%O_2. The used filler metal was OK Autorod 16.95 wire with the diameter of 0.8 mm and 1.6 mm, chemical composition of which is listed below in Table 1.2.

Table 1.2. Chemical composition of OK Autorod 16.95 wire, % mas.

C	Si	Mn	Ni	Fe
0,2	0,7	6,5	8,5	to balance

Mechanical properties of the filler metal used to weld Armox 500T steel plates are summarised in Table 1.3.

Table 1.3. Mechanical properties of OK Autorod 16.95 filler metal

Tensile strength R_m (MPa)	Yield strength $R_{p0.2}$ (MPa)	Unit elongation A_5 (%)	Impact strength KCV (J)	Hardness HBW
640	450	41	130 (+20°C)	300–340

With the use of experimentally identified welding parameters, the following joints were made:
● butt joints of 8-mm and 17-mm thick Armox 500T steel plates with the use of butt welds;
● tee joints of 8-mm thick steel plates with the use of fillet welds;
● corner joints of 17-mm thick steel plates with the use of butt welds;
● butt and corner welded joints of 17-mm thick steel plates with backing.

3. Research results and discussion

From welded joints of Armox 500T steel plates, metallographic sections were prepared with the use of grinding and mechanical polishing of transverse cross-sections of the joints and etching in Kalling's reagent. Examination of macrostructure and microstructure of the joints was carried out with the use of Neophot 2 optical metallographic microscope.

Examples views of macrostructure and microstructure from different areas of the welded tee joints and butt joints of 8-mm thick Armox 500T steel plates are shown in Figures 1.2 and 1.3.
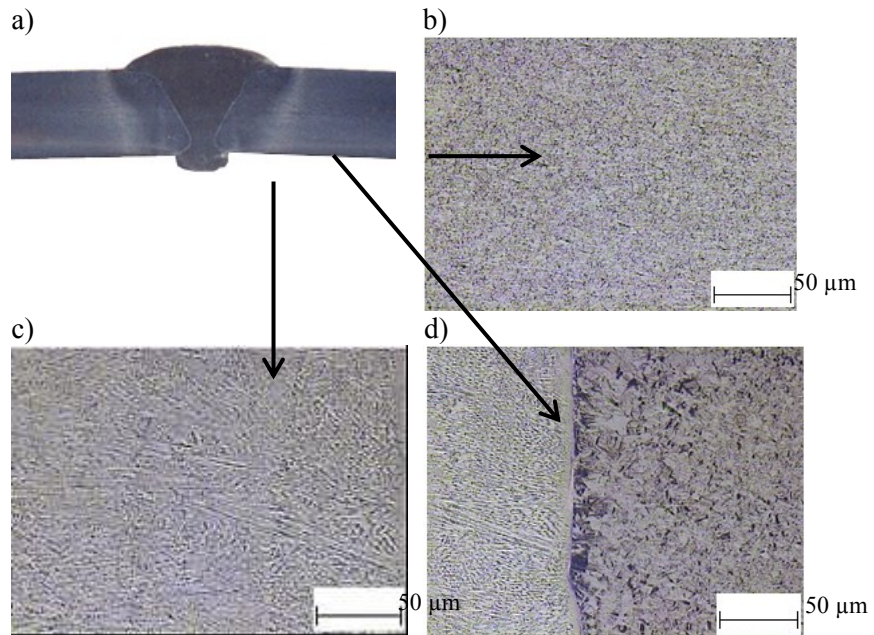
Fig. 1.2. A welded butt joint of 8-mm thick Armox 500T plates: (a) macrostructure; (b) microstructure of the parent material (PM); (c) microstructure of the weld; (d) microstructure in the weld–HAZ area
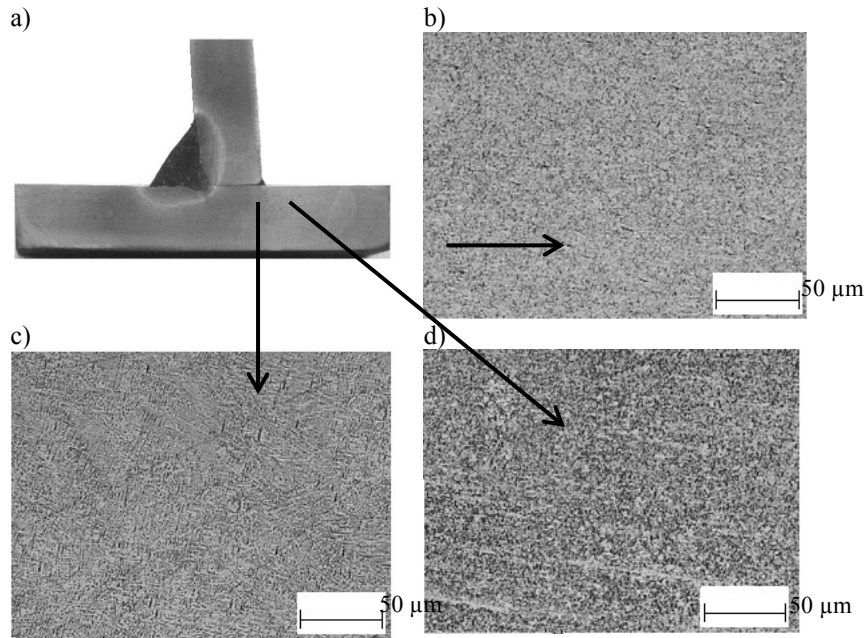
Fig. 1.3. A welded tee joint of Armox 500T steel plates made with the use of one-sided fillet weld: (a) macrostructure; (b) microstructure of the parent material (PM); (c) microstructure of the weld; (d) microstructure in the HAZ area

Figure 1.4 shows an example macrostructure of a welded corner joint corner joint of 17-mm thick Armox 500T steel plates with a backing which was fixed with the use of fillet welds.

Fig. 1.4. Macrostructure of a welded tee joint of 17-mm thick Armox 500T steel plates with backing

Welded joints of 8-mm and 17-mm thick Armox 500T steel plates have fine dendritic grains and narrow heat affected zone with grains with the size of

10–25 µm. The parent material consist of very fine (5–10 µm) grains of tempered martensite.

3.1. Macrostructure and distribution of hardness values on transverse cross-sections of welded joints

Measurements of hardness of the welded joints were carried out with the use of Zwick/Roell ZHV10 Vickers (HV10) hardness testing machine. HV10 hardness values were measured on transverse sections of welded butt joints, corner joints, and tee joints of Armox 500T steel plates with the thickness of 8 mm and 17 mm. Hardness of welded joints was measured along two lines designated A and B. Line A run at the distance of about 2 mm from the plate surface, on the face-of-weld side, while line B was drawn at the distance of about 2 mm from the plate surface, on the root-of-weld side. Additionally, for the joints welded with backings, hardness was measured along lines C and D. Figures 1.5–10 illustrate macrostructure of welded joints together with plots representing distribution of hardness values on transverse cross-sections of the joints.

a)
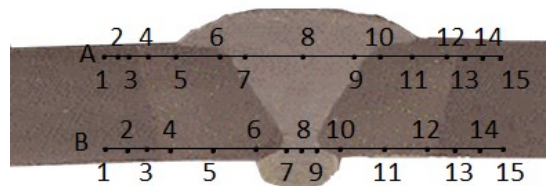
b)

Fig. 1.5. (a) Macrostructure and (b) hardness value distribution on transverse cross section of the welded butt joint of 8-mm thick Armox 500T steel plates

a)

b)
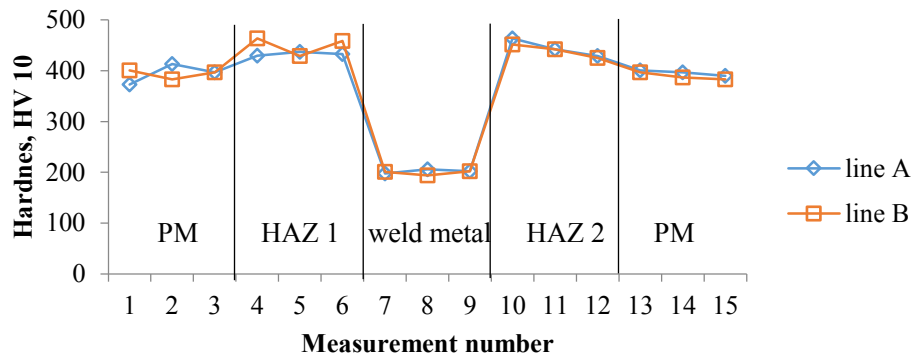
Fig. 1.6. (a) Macrostructure and (b) hardness value distribution on transverse cross section of the welded butt joint of 17-mm thick Armox 500T steel plates

a)

b)
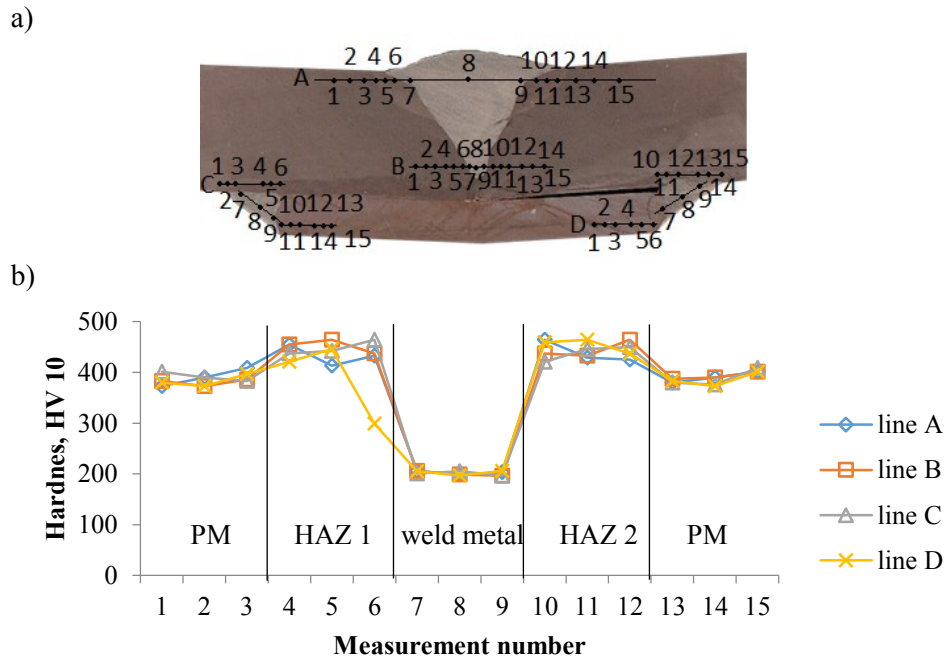
Fig. 1.7. (a) Macrostructure and (b) hardness value distribution on transverse cross section of the welded butt joint of 17-mm thick Armox 500T steel plates with backing

a)

b)
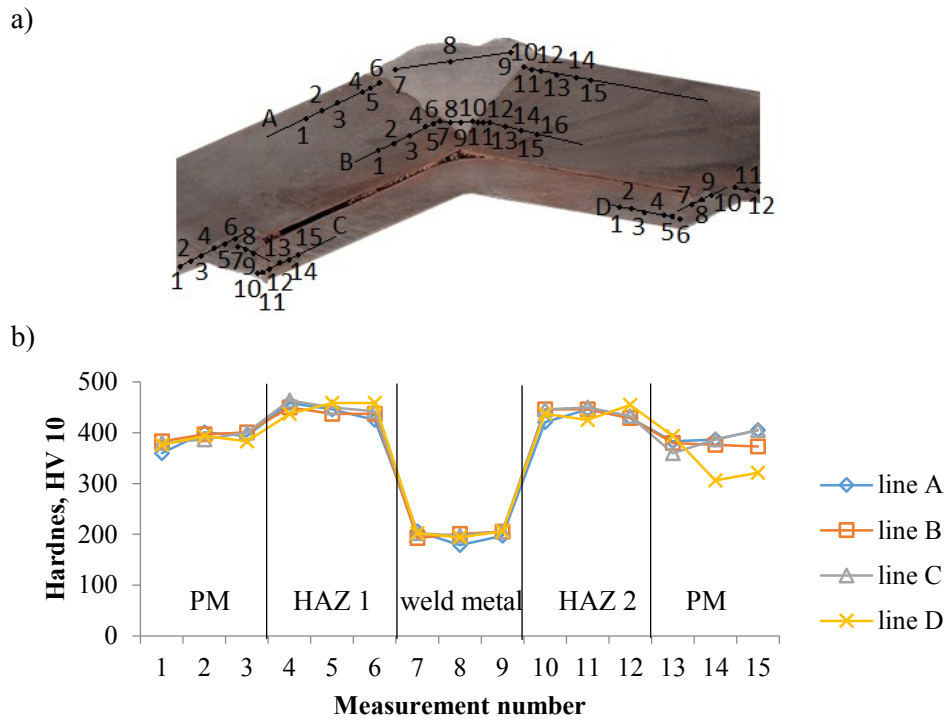
Fig. 1.8. (a) Macrostructure and (b) hardness value distribution on transverse cross section of the welded corner joint of 17-mm thick Armox 500T steel plates with backing

13

a)
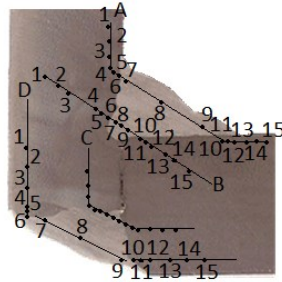
b)
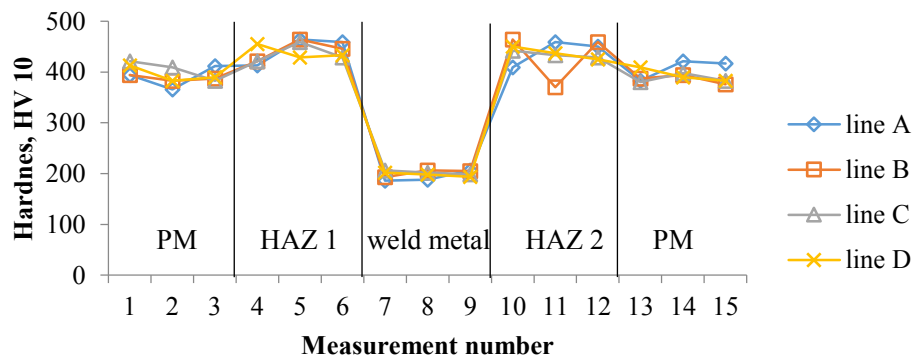
Fig. 1.9. (a) Macrostructure and (b) hardness value distribution on transverse cross section of the welded corner joint of 17-mm thick Armox 500T steel plates made with the use of two fillet welds
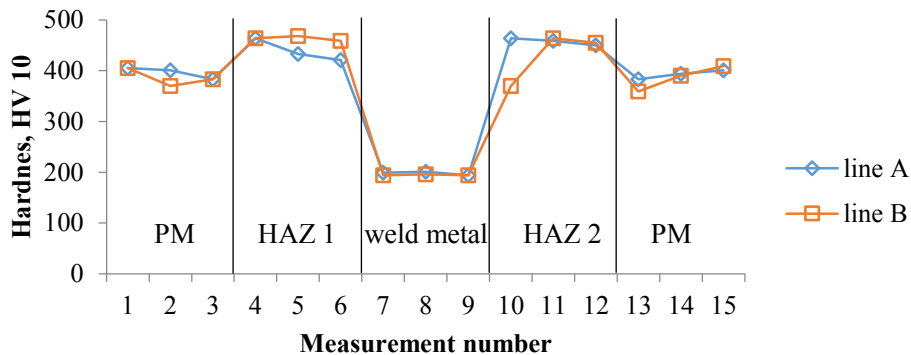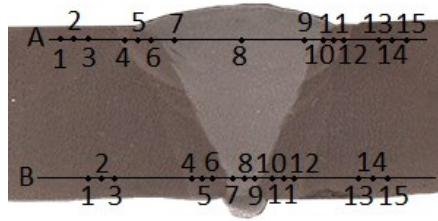
14

a)

b)
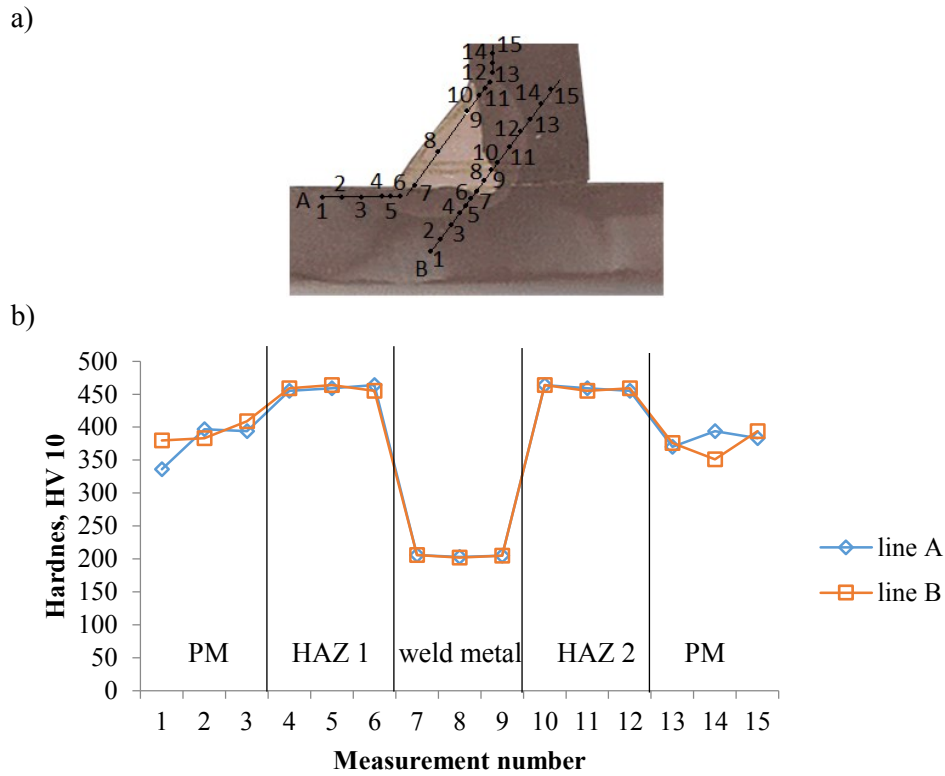
Fig. 1.10. (a) Macrostructure and (b) hardness value distribution on transverse cross section of the welded tee joint of 8-mm thick Armox 500T steel plates made with the use of fillet weld

All the analysed welded joints are characterised with a three-zone structure comprising the parent material (PM) with hardness on the average level of about 400HV10, a narrow HAZ with hardness on the level of about 450HV10, and the weld zone with hardness two times less than hardness of the parent material.

3.2. Technological process instructions for welding 8-mm and 17-mm Armox 500T steel plates

Based on results of the study on welded joints of Armox 500T steel plates with the thickness of 8 mm and 17 mm, welding instructions for individual joint types have been developed. Figures 1.11–1.16 present instructions for the process of welding the steel plates with the use of MAG method.

Preparation and cleaning method: thermal/mechanical cutting and machining of edges, shot peening	
Base material grade: ARMOX 500T /3.2 as per CR ISO 15608/	

Welding method: 135 (MAG puls)	Material thickness (mm): 8
Metal transfer method: fine droplet / pulsed arc	Outer diameter (mm): —
Joint and weld type: P BW (welded butt joint of sheet metal) 8 Y	Welding position: PA (Flat / Downhand)

Welding preparation details (a sketch):	
Drawing of the joint	Welding sequence

$t = 8$
$\alpha = 50–60^\circ$
$b = 2–3$ mm
$c = 1$ mm

Bead	Method	Filler Metal Ø (mm)	Current Intensity (A)	Voltage (V)	Current type & polarity	Wire Supply Rate (m/min)	Welding rate (cm/min)	Qty of heat introduced (kJ/mm)	Metal Flow type
1 2	135	1.0	76 170	18.5 25.5	DC (+)	5.0 9.5	10 15	0.68 1.39	Fine droplet / pulsed arc

Filler metal: solid wire	Filler metal class: EN 12072: G 18 8 Mn; AWS A5.9: ER 307 Si
Manufacturer's designation: OK Autorod 16.95 (ESAB)	

Gas: EN 439: M13 (98%Ar, 2%O_2)	Gas flow rate: 10–15 l/min
Gouging / backing details: without gouging or backing	

Preliminary heating-up temperature: min 15°C	Inter-bead temperature: max 100°C
Thermal treatment after welding: not required	
Additional information: beads No. 1–2 — right-to-left run; torch position angle 75–90°; wire stick-out 15 mm	

Fig. 1.11. Technological process instruction for welding butt joints of 8-mm thick Armox 500T steel plates

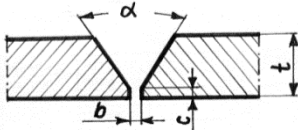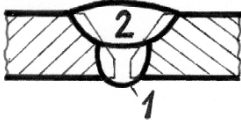|									
table below									

Preparation and cleaning method: thermal/mechanical cutting and machining of edges, shot peening	
Base material grade: ARMOX 500T /3.2 as per CR ISO 15608/	

Welding method: 135 (MAG puls)	Material thickness (mm): 17
Metal transfer method: fine droplet / pulsed arc	Outer diameter (mm): —
Joint and weld type: P BW (welded butt joint of sheet metal) 17 Y	Welding position: PA (Flat / Downhand)

Welding preparation details (a sketch):	
Drawing of the joint	Welding sequence

$t = 17$
$\alpha = 45\text{–}50º$
$b = 2\text{–}3$ mm
$c = 1$ mm

Bead	Method	Filler Metal Ø (mm)	Current Intensity (A)	Voltage (V)	Current type & polarity	Wire Supply Rate (m/min)	Welding rate (cm/min)	Qty Of Heat Introduced (kJ/mm)	Metal Flow type
1	135	1.2	80	19.5	DC (+)	3.8	10.0	0.93	fine droplet / pulsed arc
2			230	27.5		9.0	19.3	2.96	
3			230	27.5		8.8	21.2	1.79	
4			225	27.2		8.6	18.0	2.04	

Filler metal: solid wire	Filler metal class: EN 12072: G 18 8 Mn ; AWS A5.9: ER 307 Si
Manufacturer's designation:	OK Autorod 16.95 (ESAB)
Gas: EN 439: M13 (98%Ar, 2%O_2)	Gas flow rate: 10–15 l/min

Gouging / backing details: without gouging or backing	
Preliminary heating-up temperature: min 15ºC	Inter-bead temperature: max 100ºC

Thermal treatment after welding: not required	
Additional information: beads No. 1–2 — right-to-left run; torch position angle 75–90º; wire stick-out 15 mm	

Fig. 1.12. Technological process instruction for welding butt joints of 17-mm thick Armox 500T steel plate
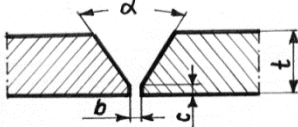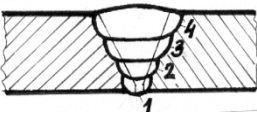
Preparation and cleaning method: thermal/mechanical cutting and machining of edges, shot peening		

Base material grade: ARMOX 500T /3.2 as per CR ISO 15608/	

Welding method: 135 (MAG puls)	Material thickness (mm): 8
Metal transfer method: fine droplet / pulsed arc	Outer diameter (mm): —
Joint and weld type: P FW (welded tee joint of sheet metal) a5	Welding position: RB (Horizontal-Vertical)

Welding preparation details (a sketch):	
Drawing of the joint	Welding sequence

$t_1 = 8$ mm
$t_2 = 8$ mm

Bead	Method	Filler Metal Ø (mm)	Current intensity (A)	Voltage (V)	Current Type & polarity	Wire Supply Rate (m/min)	Welding Rate (cm/min)	Qty of Heat introduced (kJ/mm)	Metal Flow type
1	135	1.0	190	28	DC (+)	11.5	31	0.82	fine droplet / pulsed arc

Filler metal: solid wire	Filler metal class: EN 12072: G 18 8 Mn ; AWS A5.9: ER 307 Si
Manufacturer's designation:	OK Autorod 16.95 (ESAB)

Gas: EN 439: M13 (98%Ar, 2%O$_2$)	Gas flow rate: 10–15 l/min

Gouging / backing details: without gouging or backing	

Preliminary heating-up temperature: min 15°C	Inter-bead temperature: max 100°C

Thermal treatment after welding: not required	

Additional information: bead No. 1– right-to-left run; torch position angle 75–90°; wire stick-out 15 mm	

Fig. 1.13. Technological process instruction for welding tee joints of 8-mm thick Armox 500T steel plates with fillet welds

Preparation and cleaning method: thermal/mechanical cutting and machining of edges, shot peening								

Preparation and cleaning method:								
thermal/mechanical cutting and machining of edges, shot peening								

Preparation and cleaning method:
thermal/mechanical cutting and machining of edges, shot peening

Base material grade:
ARMOX 500T /3.2 as per CR ISO 15608/

Welding method: 135 (MAG puls)	Material thickness (mm): 17
Joint and weld type: P BW (welded butt joint of sheet metal) V	Welding position: PA (Flat / Downhand)

Welding preparation details (a sketch):

Drawing of the joint	Welding sequence
$\alpha = 32°$ $t = 17$ mm $c = 2$ mm $e = 6$ mm $f = 27.5$ mm	

Bead	Method	Filler Metal Ø (mm)	Current intensity (A)	Voltage (V)	Current type & polarity	Wire Supply Rate (m/min)	Welding Rate (cm/min)	Quantity Of Heat Introduced (kJ/mm)
1 2 3	135	1,2	220–240 220–240 215–235	27–28 27–28 26.7–27.7	DC (+)	8.8–9.2 8.6–9.0 8.4–8.8	17–24 18–26 15–22	1.2–1.9 1.1–1.8 1.2–2.0

Filler metal: solid wire	Filler metal class: EN 12072: G 18 8 Mn; AWS A5.9: ER 307 Si
Manufacturer's designation:	OK Autorod 16.95 (ESAB)
Gas: EN 439: M13 (98%Ar, 2%O$_2$)	Gas flow rate: 10–16 l/min

Gouging / backing details:
with retained metal backing

Preliminary heating-up temperature: min 15°C/50°C	Inter-bead temperature: max 100°C

Thermal treatment after welding:
not required

Additional information: left-to-right run — bead No. 1, right-to-left run — weave beads No. 2–3; torch position angle 75–90°; wire stick-out 15 mm

Fig. 1.14. Technological process instruction for welding butt joints of 17-mm thick Armox 500T steel plates with backing
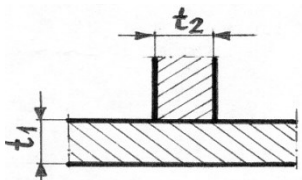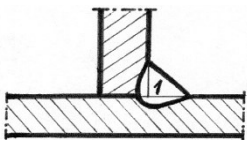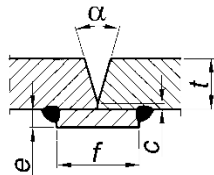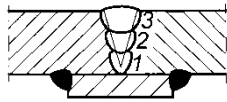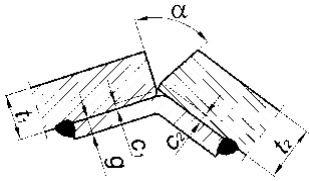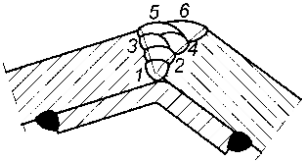
Preparation and cleaning method:
thermal/mechanical cutting and machining of edges, shot peening

Base material grade:
ARMOX 500T /3.2 as per CR ISO 15608/

Welding method: 135 (MAG puls)	Material thickness (mm): 17

Joint and weld type: P FW (corner welding of sheet metal)	Welding position: PA (Flat / Downhand)

Welding preparation details (a sketch):	
Drawing of the joint	Welding sequence

$\alpha = 32^\circ$
$t_1, t_2 = 17$ mm
$c_1, c_2 = 2$ mm
$g = 6$ mm

Bead	Method	Filler Metal Ø (mm)	Current intensity (A)	Voltage (V)	Current Type & polarity	Wire Supply Rate (m/min)	Welding rate (cm/min)	Quantity Of Heat Introduced (kJ/mm)
1			220–240	27–28		8.8–9.2	17–24	1.2–1.9
2	135	1.2	220–240	27–28	DC (+)	8.8–9.2	17–24	1.2–1.9
3–4			215–235	27–28		8.6–9.0	18–26	1.1–1.8
5–6			215–235	26.7–27.7		8.4–8.8	15–22	1.2–2.0

Filler metal: solid wire	Filler metal class: EN 12072: G 18 8 Mn ; AWS A5.9: ER 307 Si

Manufacturer's designation:	OK Autorod 16.95 (ESAB)

Gas: EN 439: M13 (98%Ar, 2%O_2)	Gas flow rate: 10 ÷ 16 l/min

Gouging / backing details:
with retained metal backing

Preliminary heating-up temperature: min 15°C/50°C	Inter-bead temperature: max 100°C

Thermal treatment after welding:
not required

Additional information: right-to-left run, string beads No, 1, 2–6 ; torch position angle 75–90°; wire stick-out 15 mm

Fig. 1.15. Technological process instruction for welding angled joints of 17-mm thick Armox 500T steel plates with backing

20

Preparation and cleaning method: thermal/mechanical cutting and machining of edges, shot peening								

Preparation and cleaning method: thermal/mechanical cutting and machining of edges, shot peening
Base material grade: ARMOX 500T /3.2 as per CR ISO 15608/

Welding method: 135 (MAG puls)	Material thickness (mm): 17
Joint and weld type: P FW (corner welding of sheet metal)	Welding position: PB (Horizontal-Vertical)

Welding preparation details (a sketch):	
Drawing of the joint	Welding sequence

$t_1, t_2 = 17$ mm
$b = 0–1$ mm
$e = (8 \pm 1)$ mm

Bead	Method	Filler Metal Ø (mm)	Current intensity (A)	Voltage (V)	Current type & polarity	Wire Supply Rate (m/min)	Welding Rate (cm/min)	Quantity Of Heat Introduced (kJ/mm)
1	135	1.0	190–210	27–29	DC (+)	11–12	19–21	1.1–1.5
2–3							22–24	1.3–1.3
4							19–21	1.1–1.5
5–6							24–26	0.9–1.2

Filler metal: solid wire	Filler metal class: EN 12072: G 18 8 Mn ; AWS A5.9: ER 307 Si
Manufacturer's designation:	OK Autorod 16.95 (ESAB)

Gas: EN 439: M13 (98%Ar, 2%O_2)	Gas flow rate: 10–15 l/min

Gouging / backing details: without gouging or backing

Preliminary heating-up temperature: min 15ºC/50ºC	Inter-bead temperature: max 100ºC

Thermal treatment after welding: not required
Additional information: (right-to-left run, string beads No. 1, 2–6 ; torch position angle 75–90º; wire stick-out 15 mm)

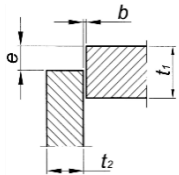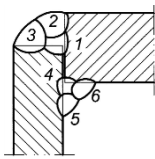Fig. 1.16. Technological process instruction for welding angled joints of 17-mm thick Armox 500T steel plates with two fillet welds

4. Summary and conclusion

Thermally hardened pieces of Armox 500T steel plates with thickness of 8 mm and 17 mm were welded by means of MAG method with the use of pulsating arc in the shield of gas containing 98%Ar and 2%O_2. The Armox 500T steel is classified as hardly weldable material with the carbon equivalent value CEV ≈ 0.75%.

The values of parameters for the process of welding such plates developed as part of the present study with the use of filler metal in the form of wire marketed under trade name OK Autorod 16.95 guarantee obtaining good quality welded joints. The joints made according to instructions shown in Figures 1.11–1.16 do not have any cracks and are characterised with narrow heat-affected zone with hardness by about 10% higher than hardness of the parent material hardness of which is on the level of about 400 HV10.

Based on results of the study concerning the course of the process of welding thick Armox 500T steel plates, the following conclusions may be drawn:

● The use of MAG welding method in the atmosphere Ar + 2%O_2 with the use of electric current with intensity in the range 80–220 A, arc voltage in the range 19–28 V, welding rate in the range 10–18 cm/min, gas flow rate in the range 10–15 l/min, and filler metal (OK Autorod 16.95 wire) feeding rate in the range 3.8–8.6 m/min to weld such armour steel plates, results in welded joints of good quality.

● The welded joints of 8-mm and 17-mm thick plates made as described above are characterised with a three-zone structure with narrow HAZ hardness of which remains on the level of about 440 HV10, whereas the weld shows high impact strength and hardness lower by about a half.

References

[1] Starzewski L., Szczęch S., Tudyka D. (2010). "Badania stali pancernych w aspekcie ich skuteczności ochronnej" [*Examination of armours steels from the point of view of their protection effectiveness*]. Prace IMŻ 1

[2] Szczęch S. (2000): "Badania metaloznawcze, wytrzymałościowe i próby balistyczne blach pancernych o grubości 2–20 mm" [*Metal science and strength examination and ballistic tests of 2–20-mm thick armour plates*]. A report on research project No. PC-4753/HPT/01/2000, Stalowa Wola

[3] Starczewski L., Szczęch S. (2001): "Opracowanie i wdrożenie do produkcji nowego gatunku stali na osłony balistyczne pojazdów wojskowych i sprzętu uzbrojenia" [*Development and industrialisation of a new grade of steel for ballistic shields of military vehicles and armament equipment*]. A final report on realisation of targeted project No. 4753, Stalowa Wola-Sulejówek

[4] Starczewski L., Garbarz B., Stępień J., Ujma J., Ujma K., Cierniak H. (2008): "Właściwości mechaniczne i odporność balistyczna blach pancernych klasy HCM 480 MILAR produkcji krajowej" [*Mechanical properties and ballistic resistance of*

class HCM 480 MILAR domestically manufactured armour plates]. WAT Monograph "Scientific aspects of armament and safety technology", Warszawa

[5] Tudyka D., Starczewski L., Szczęch S. (2009): "Wprowadzenie do produkcji KTO Rosomak kadłuba z elementów wykonanych ze stali pancernych w gat. 30PM i PM 450 produkcji HSWHSJ S.A." [*Industrialisation of a body made of grade 30PM and PM 450 armour steel manufactured by HSWHSJ S.A. for KTO Rosomak*]. A final report on realisation of targeted project No. 148515/C-T-00/2008, Siemianowice Śląskie–Stalowa Wola– Sulejówek

[6] HSW-HSJ S.A. Company research projects 2008–2009.

[7] Starczewski L. (2009): "Porównawcze badania ostrzałem prototypowych blach w gat. 30 PM i PM 450 z blachami Armox 500T i 440T oraz wyznaczenie ich granicy balistycznej *V*50" [*Comparative shooting tests of prototype grade 30 PM and PM 450 plates versus Armox 500T and 440T plates and determination of their ballistic limit V50*]. Report WITPiS No. 27/ZE/2009, Sulejówek

[8] Stępień J. (2000): "Wykresy CTPc stali w gat. 20 PM i 30 PM" [*Isothermal transformation diagrams of grade 20 PM and 30 PM steel*]. A IMŻ study for the targeted project No. 4753, Gliwice

Chapter 2.

Andrzej TRYTEK[1*]
Mirosław TUPAJ[1]
Antoni Władysław ORŁOWICZ[1]
Mikołaj KORZENIOWSKI[2]

A STUDY ON THE EFFECT OF SUBSTRATE SURFACE GEOMETRICAL STRUCTURE ON QUALITY OF COLLISION WITH POWDER PARTICLE IN THERMAL SPRAYING PROCESS

Abstract
The paper presents results of a study on collisions of powder particles with substrate in the course of thermal spraying with a metallic powder. The research included examination of geometrical structure of both substrate and sprayed coatings and microscopic observation of individual collisions of powder particles with the substrate. An attempt was made to describe the mechanism of collision of powder particles with substrate in the course of spray coating of surfaces with diversified geometrical structure corresponding to as-delivered after sandblasting conditions.

Keywords:
metallic powder, thermal spraying, substrate, geometrical structure, microscopic observation

1. Introduction

Metallic and ceramic powders are commonly used in incremental technologies used for rapid prototyping and coating in fabrication of prototype models, cores, and metal moulds. A metal powder is melted by concentrated stream of heat, e.g. laser or electron beam [1, 2]. Other applications of powders include repair of defects with the use of the powder padding technology or application of coatings by thermal spraying [3–8].

The material intended for application by way of thermal spraying may have the form of wire or powder which melts in the spraying flame. Thermal spraying

---
[1] Rzeszow University of Technology, al. Powstańców Warszawy 12, 35-959 Rzeszów, Poland
[2] BorgWarner Rzeszow Sp. z o.o., Jasionka 950B, 36-002 Jasionka, Poland
* e-mail: trytek@prz.edu.pl

offers the possibility to control both chemical and phase composition of the obtained coating. This allows to apply coatings of any material on any substrate. By controlling parameters of the process (e.g. current intensity, distance between torch and substrate, torch displacement speed) it is possible to apply coatings with large thickness on damaged or worn-out components [9].

Thermally sprayed coatings are used in virtually all industries and their individual branches as either decorative or protective surface finish applied to safeguard substrate against corrosion and high temperatures. Industrial applications of thermal spraying include also renovation, and in medical practice, thermally sprayed coatings are applied to hip joint implants. In household appliances, thermally sprayed coatings are applied on heating plates, steam irons, kitchenware, and cutting tools [10].

2. Thermal spraying

In the course of thermal spraying, heated up and molten particles of the coating material are given very high kinetic energy enabling them to adhere very well to the substrate. Therefore it is very important to prepare substrate properly before thermal spraying in order to cleanse it of contaminants, oxides, and, first of all, to give the surface the appropriate roughness.

Quality of applied coatings and layers depends on shape and size of powder particles, particle speed, temperature of particle and substrate, and geometrical structure of the latter. In industrial practice, and especially in case of renovation of geometrically complex components with the use of thermal spraying, an additional criterion is the shape of surface of the coated object. Small spaces as well as irregular and inclined walls complicate the process of spray coating. As a result of collision of first particles with substrate, the material crumbled or bounced off the sprayed surface may result in creation of areas with large quantity of oxides, porosity, and discontinuities on the substrate-sprayed coating boundary which would contribute to decrease of strength of the coating and its adherence to the substrate [18–20].

Presence of oxides in sprayed layers increases susceptibility of finished coatings to cracking. The mechanism responsible for defects of that type is occurrence of stresses between oxides and molten material of the coating as a result of different values of the coefficient of thermal linear expansion. Such coating are also characterized with elevated susceptibility to delamination [20].

A process parameter of fundamental importance in case of repairs or renovations with the use of thermal spraying is the condition of substrate. For this reason, an attempt was made to examine the mechanism of collision of a powder particle with substrate characterized with a diversified geometrical structure of its surface.

3. Examination of particle-substrate collisions

For the purpose of examination of the phenomena occurring in the course of collisions of individual particles of the sprayed powder with substrate material, specimens of two types were prepared. The first specimen was a steel plate in as-delivered condition after cleaning in an ultrasonic cleaner. The second substrate specimen was a steel plate after sandblasting with the use of a stream of abrading (alumina EFK930 with grain size 130–180 μm) supplied in air jest under pressure of 6 bar.

Both types of specimens were sprayed, in one pass, with spherical (diameter 10–50 μm) powder with the following composition: Ni 8%, C 4%, Cr to balance (Fig. 2.1).

The spraying was carried out on robotized Sulzer Metco system, equipped with IRB 2400 robot (ABB) and F4-MB-HBS plasma gun (FST) cooperating with Twin-120-A/H powder feeders volumetrically supplying the plasma gun with powder (Fig. 2.2).
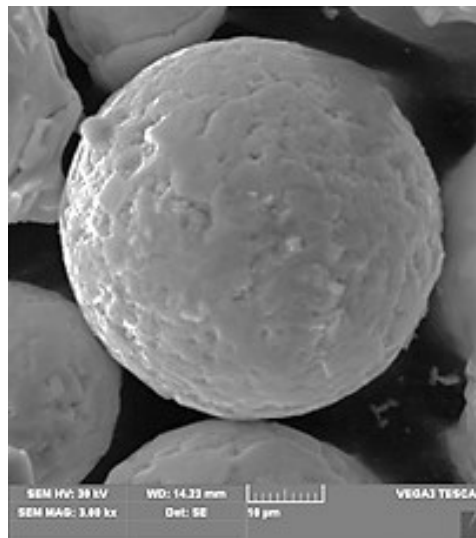

Fig. 2.1. Image of a spraying powder particle

Fig. 2.2. Image of the Sulzer Metco plasma spraying system: the booth
with ABB robot

On specimens both prepared for and after thermal spraying, examination of geometrical structure of surface was carried out (Fig. 2.3). The measurements were carried out on a measuring setup equipped with stationary profilometer T8000 by Hommel Etamic allowing to take measurements in 3D system with the use of TKU300 measuring tip advanced at rate $V_t = 0.5$ mm/s over a measurement area 3 mm × 3 mm. To analyze the phenomena of interest, typical surface profile parameters were adopted, namely S_z (maximum surface height), S_a (arithmetic average surface height), and S_t (profile height) (Fig. 2.3).
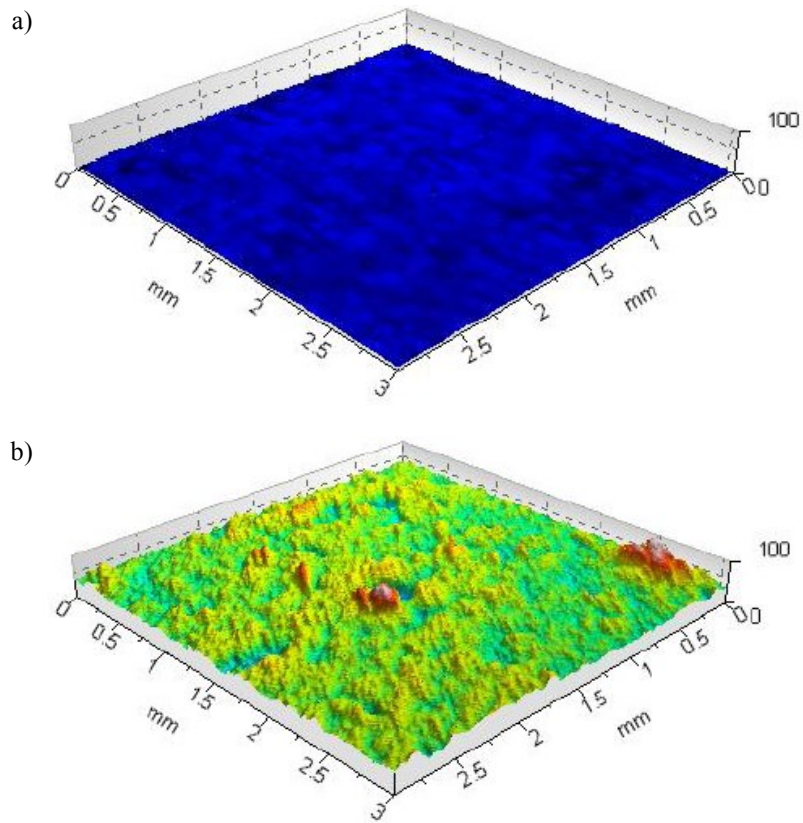
Fig. 2.3. Geometrical structure of steel specimens in (a) as-delivered and (b) after sandblasting condition

A view of as-delivered and sandblasted steel specimens after thermal spraying is presented in Figure 2.4. The pass sprayed onto the as-delivered substrate (Fig. 2.4a) is uneven and scattered. The pass applied to the sandblasted substrate (Fig. 2.4b) is straight and uniform. Geometrical structure of specimen surfaces after thermal spraying is shown in Figure 2.5.
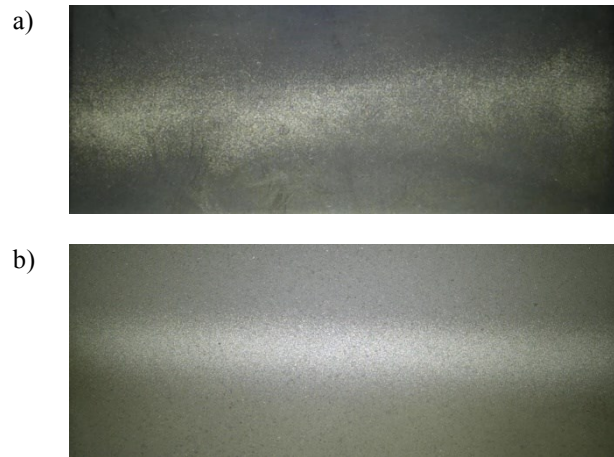
a)

b)

Fig. 2.4. Image of steel specimens after thermal spraying with the substrate (a)
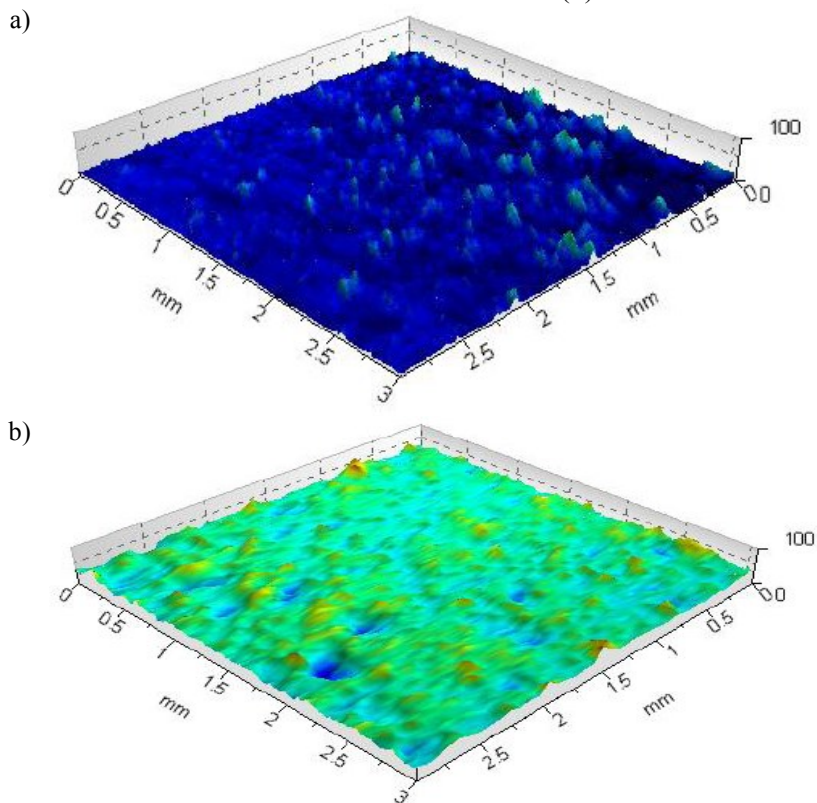in as-delivered condition and (b) sandblasted

a)

b)

Fig. 2.5. Image of steel specimens after thermal spraying. Geometrical structure
of surface (a) in as-delivered condition and (b) after sandblasting

Table 2.1 is a summary of parameters characterizing geometrical structure of steel specimen surfaces depending on condition of the substrate and the same parameters characterizing thermally sprayed surfaces.

Table 2.1. Values of steel substrate surface geometrical structure parameters

Specimen initial condition		Surface geometrical structure parameter		
		S_z (μm)	S_a (μm)	S_t (μm)
As delivered	—	9.64	0.929	17.5
As delivered	after thermal spraying	45.4	3.03	54.0
after sandblasting	—	78.2	5.58	99.1
after sandblasting	after thermal spraying	67.2	4.98	77.5

Analysis of the results indicates that in case of substrate in as-delivered condition after deposition of the sprayed coating, values of the surface geometrical structure parameters increase. On the other hand, when the substrate is sandblasted and only then thermally sprayed, values of parameters S_z, S_a, and S_t decrease.

The specimens after thermal spraying were further prepared for observation with the use of MIRA 3 field emission scanning electron microscope (Tescan). Results of the observation are presented in Figures 2.6 and 2.7.
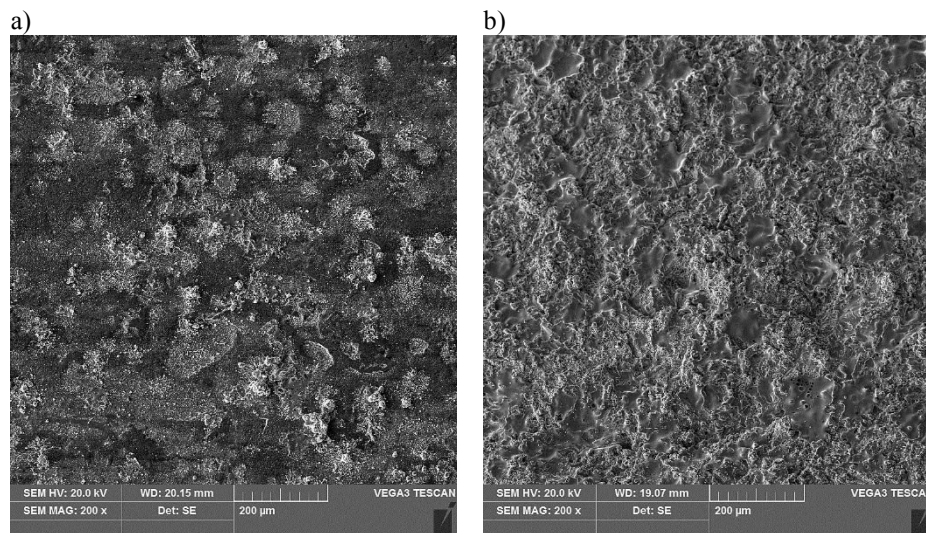
a)

b)

Fig. 2.6. Image of specimen surfaces: (a) substrate in as-delivered condition after thermal spraying; (b) substrate in as-delivered condition after sandblasting and thermal spraying
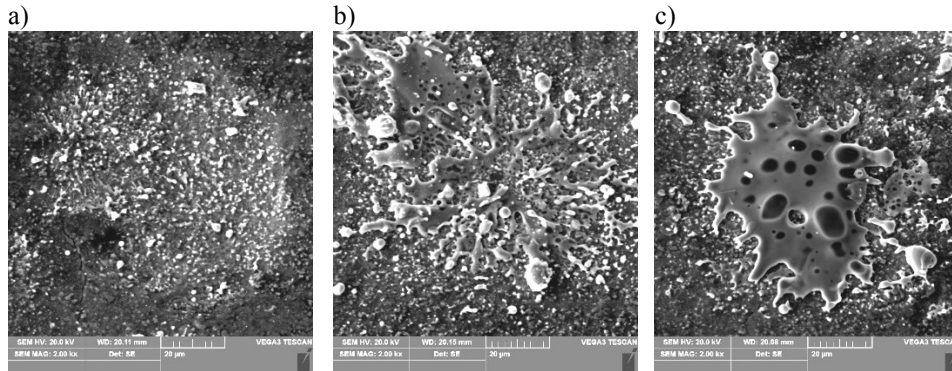
a)   b)   c)

Fig. 2.7. Image of particles after collision with substrate specimen in as-delivered condition after thermal spraying: (a) crater, (b) spattering, (c) adhesion with gas blisters

Observation of surface of the substrate specimen subject to thermal spraying in as-delivered condition (Figs. 2.4–2.8) revealed craters and other marks of particle-collisions, particles clung on to the substrate, or spattered droplets of liquid metal. On surface of the substrate specimen first sandblasted and then thermally sprayed with metallic powder, only particles clung on to the substrate or spattered droplets of liquid metal were observed. On the specimen sprayed in as-delivered conditions, the following characteristic types of collision were identified: a crater (Fig. 2.7a), a spattering (Fig. 2.7b) and adhesion with gas blisters (Fig. 2.7c). On the specimen with substrate sandblasted and then thermally sprayed, the characteristic types of collision were (Fig. 2.8a–c): particle torn apart on protruding features of substrate, adhesion to substrate, and spattering with gas blisters.

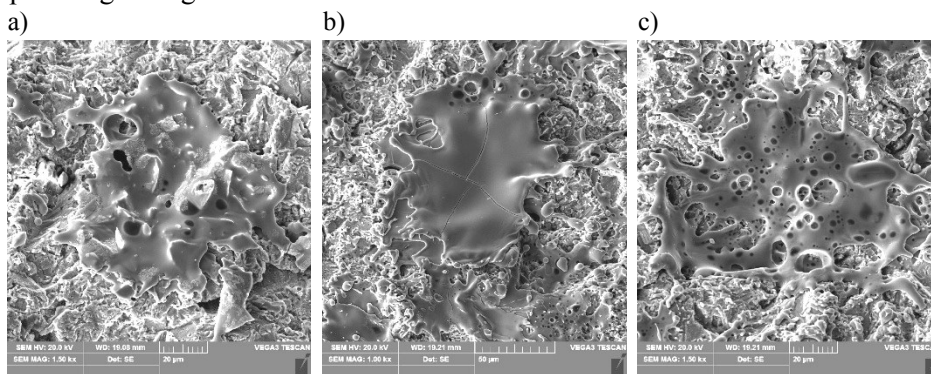a)   b)   c)

Fig. 2.8. Image of particles after collision with specimen with substrate after sandblasting and after thermal spraying: (a) particle torn apart on protruding features of substrate; (b) adhesion to substrate; (c) spattering with gas blisters

4. Summary and conclusions

Analysis of results of the performed research and literature of the subject allow to disclose the mechanism of interaction of first powder particles reaching substrate in the course of thermal spraying. Depending on its state of matter (liquid, partially molten, heated up), a particle colliding with surface of the substrate forms a crater, adheres to substrate, or crumbles [14]. During collision of with substrate, gas blisters are formed in the space under a flattening droplet [21]. Population and sizes of these gas blisters depend on parameters of the spraying process, type of material, droplet viscosity, and condition of substrate surface (temperature and roughness). Fukanuma H. and collaborators [21, 22] have carried out experimental and simulation studies on forms of particles flattened on the substrate surface. Their experimental observations of isolated particles solidified on the substrate revealed presence of furrows and grooves formed by splashed metal under surface and gas blisters in centers. Such features are consistent with what was observed in the course of the present study.

Based on results of the performed research on the mechanism of metal powder particle collisions in the course of thermal spraying onto a substrate it can be stated that:

- the condition (state of preparation) of substrate surface has an effect on the character of collision of powder particle with the substrate;
- on a substrate with surface of flat geometrical structure, individual particles form craters, get broken into fine particles, with gas blisters possibly formed under adhering particles (Fig. 2.7);
- on substrate surface after sandblasting (Fig. 2.8), particles adhere to the substrate forming a coating stretched over individual rises or spatter with gas blisters;
- torn-away fragments of particles can be strongly oxidized and may form discontinuities and porosity of the coating once adhered to substrate.

Values of the surface geometrical structure parameters (S_z, S_a, S_t) of a substrate in as-delivered condition subject to thermal spraying with no further preparation increase. This results from spattering and fragmentation of powder particles in the course of collision with specimen surface (Table 2.1 and Figs. 2.7, 2.9). The decrease of values of the parameters characterizing geometrical structure (S_z, S_a, S_t) of a substrate sandblasted and then thermally sprayed follows from the fact that molten powder particles fill craters and voids in specimens (cf. Table 2.1 and Figures 2.8, 2.10).

A schematic representation of the mechanism of collision of a metallic powder particle with substrate in as-delivered condition and after sandblasting is shown in Figures 2.9 and 2.10, respectively.

Absence of preliminary preparation of substrate contributes to fragmentation and spattering of particles as a result of collision with the material subject to spray

coating. Application of sandblasting to the substrate is favorable to adhesion of individual particles to the substrate material and reduces the number of spatters.

a)　　　　　　　　　b)　　　　　　　　　c)

Fig. 2.9. A schematic representation of the mechanism of collision of a metallic powder particle with substrate in conditions as-delivered after thermal spraying: (a) crater; (b) spattering; (c) adhesion with gas blisters
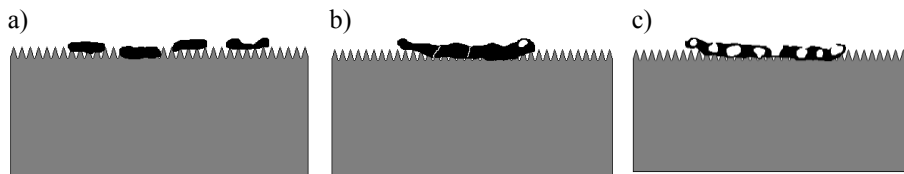
a)　　　　　　　　　b)　　　　　　　　　c)

Fig. 2.10. A schematic representation of the mechanism of collision of a metallic powder particle with substrate in condition after sandblasting and after thermal spraying: (a) particle torn apart on protruding features of substrate; (b) adhesion to substrate; (c) spattering with gas blisters

The observed collision mechanisms (especially spattering and formation of gas blisters) on substrate characterized with low values of surface geometrical structure parameters (e.g. as-delivered condition) are unfavorable. Coatings and layers prepared that way will demonstrate increased susceptibility to delamination, and in view of large quantity of oxides and gas blisters, porosity, and discontinuities, one should expect decreased strength and adherence of the coatings to substrate.

The performed study confirms the necessity to prepare the surface properly (e.g. by sandblasting) for thermal spraying and develop a technological process appropriate for spray-coating of details with complex shape, close to inner edges, between walls, or inside holes in a way counteracting occurrence of craters, blisters, and/or spattering of individual particles in these specific conditions.

References

[1] Budzik G. (2007): Possibilities of utilizing 3DP technology for foundry mould making. Archives of Foundry Engineering, Vol. 7, Issue 2, 65-68

[2] Budzik G. (2007): Properties of made by different methods of RP impeller foundry patterns. Archives of Foundry Engineering, Vol. 7, Issue 2, 83-86

[3] Karwiński A., Haratym R., Soroczyński A., Kowalski P. (2014): Comparison of Quality of Investment Castings Produced Based on the Rapid Prototyping Techniques with Products of Powder Sintering. Archives of Foundry Engineering, Vol. 14, Special Issue 3, 31-34

[4] Rahimy Y., Vahdat S.E. (2016): Repair of Structural Steel Surface Groove by Using Diffusion Welding of Pure Iron Powder. Archives of Foundry Engineering, Vol. 16, Issue 2, 105-110

[5] Opiekun Z. A., Trytek A. (2014): Cohesion and Adhesion Interlayer of the Thermal Barrier Coatings Made of Cobalt Alloy MAR-M509. Archives of Foundry Engineering, Vol. 14, Special Issue 1, 159-164

[6] www.oerlikon.com

[7] Pinkerton A.J. (2015): Advances I the modelling of lasr direct metal deposition. Journal of Laser Applications Vol. 27, No S1, February, S15001-1-7

[8] Ebrahimnia M., Malek Ghaini F. Gholizade Sh., Salari M. (2012): Effect of cooling rate and powder characteristics on the soundness of heat affected zone in powder welding of ductile cast iron. Materials and Design 33 551–556

[9] Xing Y., Li X., Zhang Y., Jiang C., Zhang W. (2016): Effect of Spray Parameters on the Splashing of Plasma-sprayed Cast Iron Particles. Journal of Wuhan University of Technology-Mater. Sci. Ed. www.jwutms.net, 399-403

[10] Mathesius A.A., Krommer W. (2009): Praxis des thermischen Spritztens. DVS Media GmbH, Dusseldorf

[11] Dudek S. (2009): Mikrostruktura i ocena właściwości barier cieplnych wykonanych metodą natryskiwania plazmowego na elementach komory silnika spalania. Rozprawa doktorska. Politechnika Rzeszowska, Rzeszów

[12] Dawon Seo Kazuhiro Ogawa (2012): Isothermal oxidation behavior of plasma sprayed MCrAlY coatings. www.intechopen.com Advanced Plasma Spray Application. Edited by Hamid Jazi, 61-82

[13] Kahraman N., Gülenç B. (2002): Abrasive wear behavior of powder flame sprayed coatings on steel substrates., Material and Design, 23, 721-725

[14] Van Steenkiste T.H., Smith J.R., Teets R.E. (2002): Aluminum coating via kinetic spray with relatively large powder particles. Surface & Coating Technology, 154, 237-252.

[15] Kuroda S., Kawakita J., Watanabe M. and Katonada H. (2008): Warn spraying a novel coating process based on high-velocity impact of solid particles., Sc.Tech. Adv. Mater., 9, 1-17

[16] Yoon S., Xiong Y., Kim H., Lee C. (2009): Dependence of initial powder temperature on impact behaviour of bulk metallic glass in a kinetic spray process. Journal of Physics D:Applied Physics, 42, 1-5.

[17] Radek N., Pliszka I., Liszewski D. (2015): Właściwości powłok wytwarzanych technologiami wykorzystującymi skoncentrowany strumień energii i ich potencjalne zastosowanie w taborze kolejowym. Problemy Kolejnictwa, Z. 166, 127-146

[18] Rupprecht Ch. (2013): Neue Methodenund Anwendungen des Thermischen Spritzens. Technische Universitat Chemnitz, Habilitations

[19] Sarikaya O. (2005): Effect of some parameters on microstructure and hardness of alumina coatings prepared by the air plasma spraying process. Surface and Coatings Technology 190, 388-393

[20] Neiser R.A., Smith M.F., Dykhuzen R.C. (1998): Oxidation in wire HVOF-sprayed steel. Term. Spray Technol. Vol. 7. No 4, 537-545

[21] Fabrication of nanoporous metallic surfaces via rapid impact and solidification of molten droplets.
http://www1.coe.neu.edu/~agouldstone/?page=research

[22] Fukanuma H., Huang R., Tanaka Y., Uesugi Y. (2009): Mathematical modeling and numerical simulation of splat cooling in plasma coatings. http://www.plasma.co.jp/about/2009-2.html

Chapter 3.

Dominik GAŁDYŃSKI[4*]
Wawrzyniec GOŁĘBIEWSKI[1]
Maciej LISOWSKI[1]

REPAIR TECHNOLOGY OF TRUCKS FRAME BEARERS

Abstract
The subject of this study is the numerical analysis and empirical studies of strength parameters of energy-consuming and load-bearing structures of vehicles subjected to longitudinal crushing, consisting in cutting off the damaged element and welding the new element in places provided for in repair technology by the vehicle manufacturer. During each panel-beating repair of frames or other reinforcements of the vehicle structure, consisting in their partial replacement, they acquire features related to the change of material and shape structure resulting from the use of welding processes. Changing these parameters related to repairs may reduce the strength properties and thus weaken the structure of the vehicle itself. The subject of the analysis was the evaluation of the influence of welding processes used during the liquidation of deformations resulting from stress influences exceeding the yield point of the material from which the element was made. As a result of the conducted research, a method for joining the elements to be replaced was proposed, which will allow to reduce the impact of the welding process on the strength parameters of the repaired structures. The analysis of numerical simulations and empirical studies on the samples confirms the assumptions made. Full verification of the suitability of the proposed method will be possible after performing the tests of the actual elements.

Keywords:
frame, profile, repair, strength, welding

---

[4] Automotive Engineering Department, West Pomeranian University of Technology, Szczecin, al. Piastów 19, 70-310 Szczecin, Poland,
[*] e-mail. dgaldynski@zut.edu.pl

1. Introduction

The subject of the article is to present an alternative, to the currently used, technique of replacement of a frame bearer construction element, most often used in the construction of trucks or off-road vehicles.

These are most often cross sections of classes I, II and III. The steel section classes classify the resistance of the element to the loss of local stability of the section walls. The PN-EN 1993-1-1 + A1,2006 standard defines four classes of steel sections I, II, III and IV, while in classes I, II and III there is no local loss of stability of section walls during axial compression.

The authors set out to develop a solution that will allow, in a simplified manner, to carry out procedures for the technology of such exchange, constituting a viable alternative to currently used repair methods. The criterion that was set implied a minimal difference in repair costs using an alternative method in relation to the conventional method, including time-consuming of such a process, the cost of adapting already existing technical facilities, that is equipment, employee training, and other costs whose adverse relationships could make the proposed solution unprofitable. In addition to the aforementioned description of the proposed repair technology, it is also important to present its limitations so that this solution can be correctly applied in the technology of repairing the vehicle's load-bearing structures.

2. Conventional method and its limitations

The vehicle's operational documentation includes, among others, a section on technology for its repair [0,0]. In many cases the technology, imposed by the vehicle manufacturer, assumes the replacement of the damaged part with a new one or a factory-repaired one without the possibility of repairing them. In other cases repairs are foreseen by molding, plastic working etc. Partial replacement is also foreseen without the need to replace it completely in case of partial damage. This study is devoted to partial replacement. Partial replacement technology, assumes the removal of the damaged part of the chassis structure of the vehicle, and inserting the repair element in this place and its permanent joining into the whole frame structure.

The idea of repair, using the regime of the developed technological process, assumes valorisation of the functionality of repaired components to the original level, without the risk of losing strength or aesthetic parameters [0,0]. The technological regime specifies the method of disassembly and assembly of replaced sections of the frame structure profile and other components of the process, such as the indication of tools for the welding machine workshop, GMAW welders, supply voltage installation, fuse covers, and the possibility of keeping the anti-corrosion warranty which is granted when purchasing a vehicle [0].
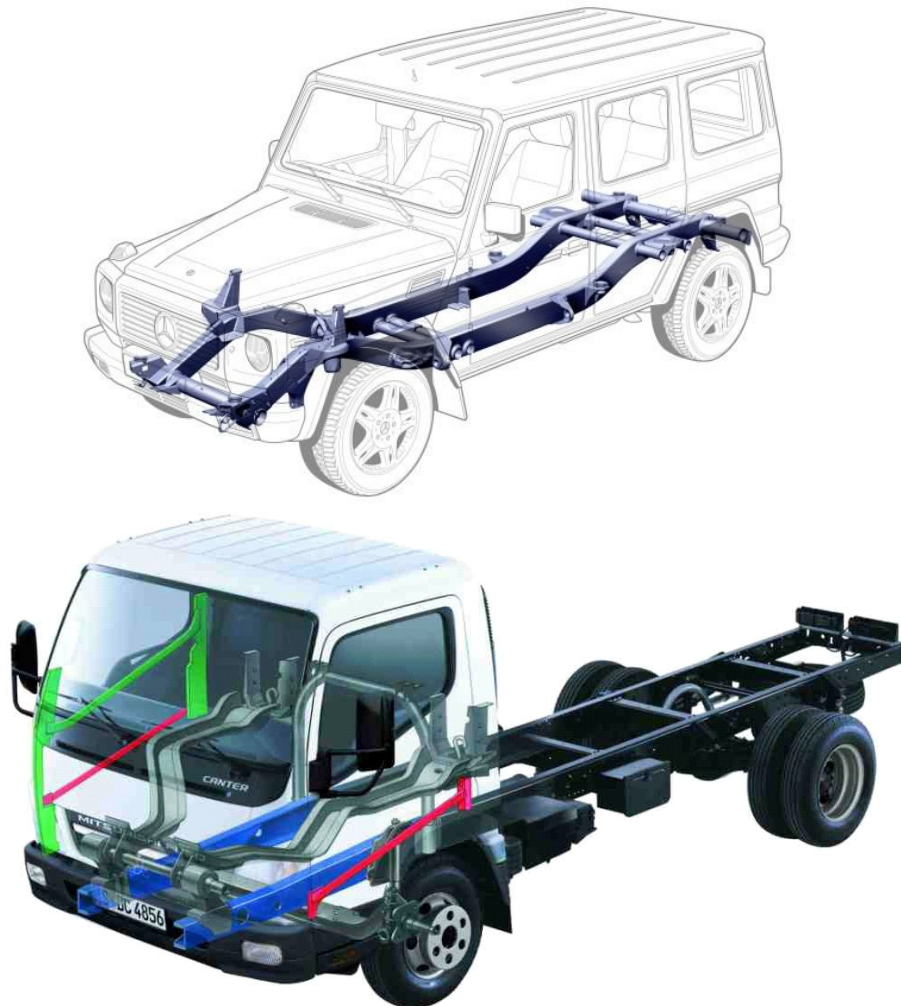
Fig. 3.1. Examples of vehicle frame bearers structures [14].

2.1. Cause of a problem

The assumptions of the process of partial replacement of the damaged profile constituting a component of the overall structure of the vehicle support frame, imply changes in the structure of the material in the zone of heat influence, inclusions, discontinuities and shape defects due to deformation caused by welding contractions [0,0,0,0]. Additionally, it should be noted that the AHSS steel, which is most commonly used in the construction of side-members in modern vehicles, is characterized by dynamics of the increase of tensile strength R_m from year to year. When in the nineties, in the era of widely used "deep-drawn" steel with R_m parameters of 150 MPa, the introduction of high-strength

steel with 200MPa parameters did not imply, at the post-production stage, problems related to the welding process, because the available welding wires G1.. 250MPa, G2.. 370 MPa,, and later G3Sil 570MPa met the criterion of adjusting the additional material (welding wire) to the level of tensile strength R_m of the parent material (welded). So nowadays, when the tensile strength R_m of AHSS steel from which the side-member frame of a modern vehicle is built oscillates in the range of 1000-1500 MPa, and sometimes 2000MPa and more [0,0,0]. Getting a connection in the context of the isomorphic strength of the structure of the repaired part seems to be an impossible condition [0]. Also the use of special-purpose welding wires with tensile strength R_m 890 MPA (e.g. A5.28 ER ... XS-X), which is used in industry, e.g. shipbuilding, with infrastructure for industrialized processes, does not allow full valorisation of the strength of the repaired element[3,0,0]. The most expected, in the light of the issues mentioned, would be to replace the damaged part of the chassis, consisting in complete replacement of the whole frame. However, this action generates significant costs, which in most cases may result in exceeding the value of the repaired vehicle - especially if it is not new, which in turn leads to unprofitability of repair and the occurrence of so-called "total damage". This scenario is not indicated because it undermines the economic sense of the repair. Therefore, it seems that the partial exchange procedure will not be discontinued, and the solution to the problem should be sought in the manner of connection, and this will be the next part of the study.

3. Preliminary - material tests

In order to recognize and define the amount of loss of strength properties of AHSS steel, in connection with the welding process carried out, high tensile strength DP steel was used for the tests, manufactured in accordance with PN-EN 10346: 2011.

3.1. Preparation of samples

The shape and dimensions of the samples for the quasi-static stretching test were made in accordance with the PN-EN ISO 4136: 2011 standard. In order to determine the parameters of strength properties of the welded joint, the face and ridge of the weld had to be sanded to the thickness of the base material. However, the determination of these parameters for the HAZ, already with a rough analysis of the R_m value used for welding a welding wire of 570 MPa, with the strength of this parameter for the base material of 931 MPa - (σ_{rz} value determined during the tensile test), cannot, using this methodology, bring the expected results. To implement the main assumption, which is to determine the coordinates of the tensile plot parameters for the HAZ, it was decided to leave the weld face and ridge unsanded for some prepared samples. In this way, by significantly increasing the cross-section of the test sample in the joint, the probability of

breaking it in the weld area was eliminated, transferring the main stress load into the HAZ area.

3.2. Welding parameters

For DP steels coated with zinc coating, the recommended welding methods are arc welding and laser beam. The producers of these steels allow the use of all arc welding methods, with particular reference to the MIG, TIG and PAW methods [5]. The genesis of a properly performed welding process is applied to the additional material, which has a higher tensile strength than the base material, however, in the case of AHSS steel, the tensile strength of the weld may be lower than the base material, due to the lack of available materials with such a high R_m [0,0,0], as well as due to the significant impact of changes in strength in the HAZ, as shown by the results of the conducted tests. The samples were obtained by welding the DP 800 material with the MIG method, buttress without chamfering the edge of the welding groove with the parameters: (PN-EN 14175: 2009)

Table 3.1. Tensile strength parameters of DP 800 steel used for testing

Method	Shielding gas mixture	Welding voltage	Welding current	Wire feeding speed	Determination of welding wire
MAG	Ar + 18% CO_2	18 V	35 Amp	2,4 m/min	G3Sil

3.3. Research position

Tensile tests were carried out on a two-column universal testing machine INSTRON 8850, equipped with a strain gauge with a measuring range of 0-250kN. The INSTRON extensometer with a 50 mm measuring base length was used to record the deformation. The tests were carried out at a beam speed of 5 mm/min.

3.4. Tensile strength test results

The graphs parameters obtained during the tests were transformed into the form of stress and real strain using the relation:

- The actual σ_{rz} stress as the ratio of the force extending the sample to the actual cross-sectional area of the sample part:

$$\sigma_{rz} = \sigma_n(1 + \varepsilon_n)$$

- The ε_n nominal deflection referred to the initial length of the sample:

$$\varepsilon_n = \frac{\Delta l}{l_0}$$

- Normal stresses:

$$\sigma_n = \frac{F}{A_0}$$

A_0 – the initial surface area of the cross section of the sample part.

- Actual deformation ε_{rz} of the tested sample:

$$\varepsilon_{rz} = \ln\left(1 + \frac{\Delta l}{l_0}\right)$$
$$\varepsilon_{rz} = \ln(1 + \varepsilon_n)$$

The obtained results of the R_m parameter are shown in Tables 3.4 and 3.5.

Table 3.2. Tensile strength test results of butt-welded joints AHSS steel type DP800 - samples torn in HAZ

No.	Sample No. 1	Sample No. 2	Sample No. 3	Average value R_m
σ_{rz} R_m[MPa]	737	712	684	711

Table 3.3. Tensile strength test results of butt-welded joints AHSS steel type DP800 - samples torn on the weld.

No.	Sample No. 4	Sample No. 5	Average value R_m
σ_{rz} R_m[MPa]	585	654	620

Table 3.4. Tensile strength parameters of DP800 steel used for testing.

	σ_{rz} $R_{p0.2}$ [MPa]	σ_{rz} R_m[MPa]	HRA
Sample No. 6	694	931	62

3.5. The results of hardness tests of base material and welded joints.

The test was performed with a static hardness tester, Rockwell HRA according to the PN-EN ISO 6508-1: 2002 standard.
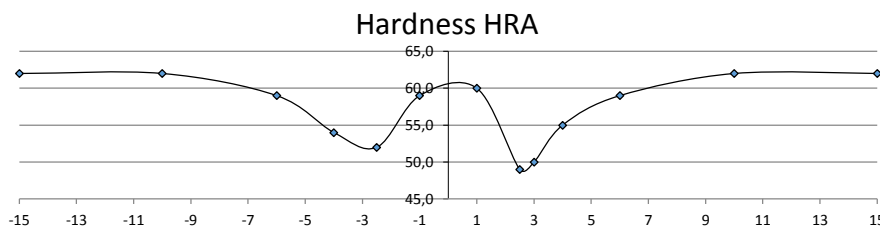

Fig. 3.2. Hardness chart of welded connection of tested steel DP800

Table 3.5. Results of the Rockwell HRA static hardness test of the welded steel DP800.

Measurement width relative to the transverse axis of the sample [mm]	-15	10	-6	-4	-2,5	-1	1	2,5	3	4	6	10	15
Hardness HRA	62	62	59	54	52	59	60	49	50	55	59	62	62

3.6. Discussing the results

As can be seen, the drop in the tensile strength of the weld joint, for the SWC area was about 25% in relation to the sample without the application of the weld, and for the samples torn on the weld 33%.

4. Modeling and numerical analysis of the structure of oneomega profile

After determining the declines in tensile strength Rm for the welded joint, a simulation was performed by which the concentration of stresses that accumulate in the weld area was visualized. To carry out the simulation, it was assumed that the model is made of isotropic steel with the following properties:: Young's modulus $E = 2,1*10^5$MPa, Poisson's number = 0,3, density = 7890 kg/m, tensile strength Rm = 931 MPa, yield point $R_{0.2}$ = 694 MPa. The results of the FEM analysis in the form of reduced stress distribution were carried out according to the Huber-Mises hypothesis. Geometric values of the proposed system were determined according to the following sizes, length 300mm, width 100mm height 61mm. The first step was to model the side-member system, taking into account the application of a weld made in a conventional manner, on which morphological changes were applied, of course in a limited range of identifiable features. Fig. 3.3 shows the geometrical changes of the introduced connection application, the shape corresponding to the profiles with high wall thickness, which led to the adoption of such a cross-section. The coordinates of the tensile tests R_m were also defined during the material tests, for each of the analyzed zones, i.e.: base material sample No. 6, HAZ sample No. 2, welds sample No. 4.
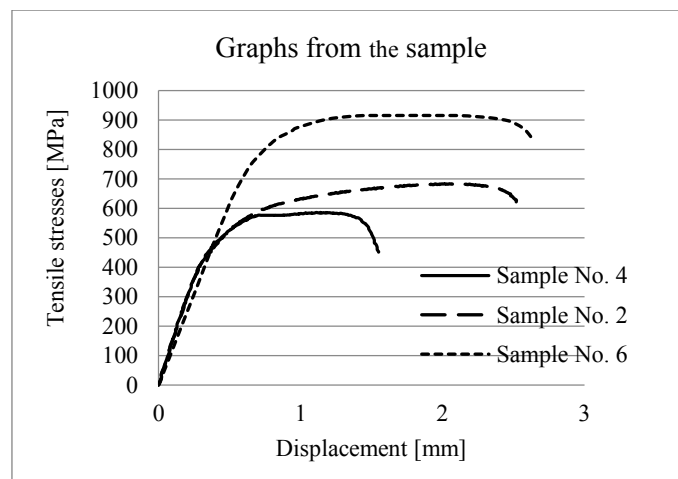

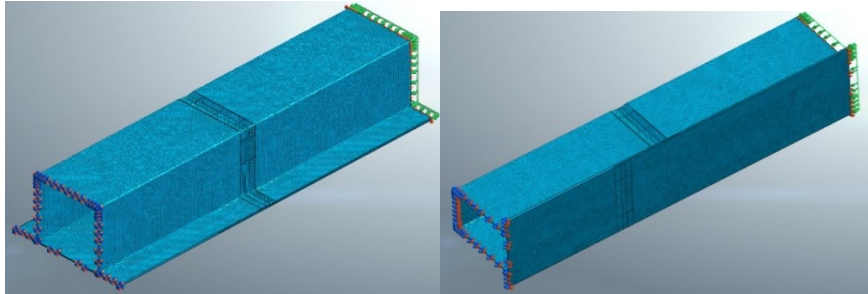Fig. 3.3. Graphs of the tensile test for the Samples No.2,4,6.

Fig. 3.4. The proposed geometric shape of the side-member and the welded connection.
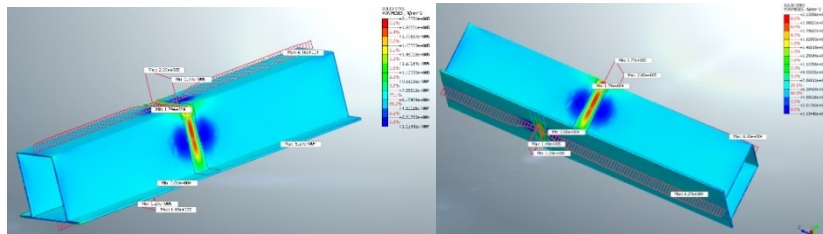

Fig. 3.5. The result of numerical analysis, showing the concentration of stresses in the areas of weld applications introduced.

4.1. Discussing the results

A clearly visible concentration of stresses at the place of the introduced weld application, shows the discussed phenomenon which is the decrease of the strength properties of the side-member as a result of morphological changes that accompany the welding process.

5. Analytical solution to the problem

The side-member profile constituting the component of the overall self-supporting structure of the vehicle chassis due to its spatial shape transfers the compressive, tensile and torsional stresses caused by bending moments caused by the normal operation of the vehicle. When dealing with a complex state of stress, this profile is subjected to constant compression, stretching and bending. Torsional stresses are omitted for simplicity. For example, when the top horizontal wall of the hat profile, due to the bending moment on the frame, is compressed and generally has stresses comparable to a one-axial-flat stress system (in simplified form). In the vertical, side walls of the profile, there are compressive stresses and tensile stresses with the neutral axis, whose "fibers" are "free" of these stresses, and in the flat and "feet" of the hat profile, these elements

are subjected to tensile stresses. However, the vehicle frame is exposed not only to stresses resulting from normal operation, but can also be subjected to significant loads not anticipated in normal operation. Using the above simplification, with a flat state of stress, they were proposed to be reduced in the area of the weld by changing the angle of the cutting line of the combined components, using the dependence [13]:

$$6_x = \frac{1}{2} 6 \, (1 + cos2\acute{\alpha}); \; 6_y = \frac{1}{2} 6 \, (1 - cos2\acute{\alpha}); \; \tau_{xy} = -\frac{1}{2} 6 \, (sin2\acute{\alpha}).$$

where:
$6 -$ *normal stresses.*
$\tau -$ *tangential stresses.*

Using the above relationships and comparing the results of the reduction of normal stresses 6 in the cross-section, along with the increment of the cutting line length, the characteristics were obtained (Fig. 6.7).
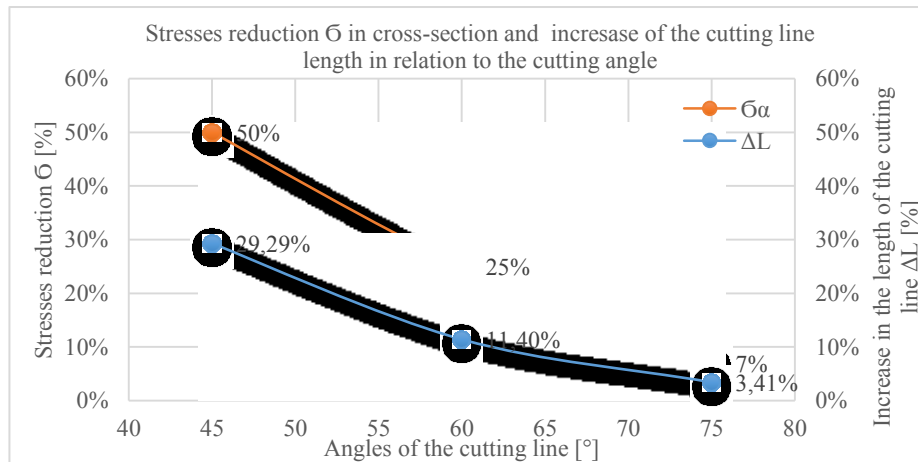

Fig. 3.6. Graph of normal stress reduction 6 in cross-section and increase of cutting line length in relation to its angle.
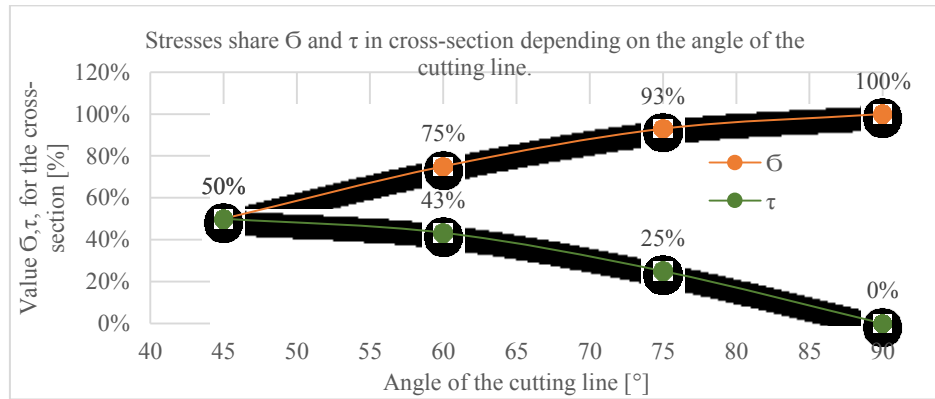
Fig. 3.7. Graph of the share of normal Ϭ and tangent τ stresses in the cross-section depending on the angle of the cutting line.

5.1. Discussing the results

It was observed that along with the change of the cutting line angle (cross-section), the share of normal stresses and tangential stresses to this cross-section change. Using this simple relationship, by changing the angle of the cutting line and performed welded connection from parallel to the cross-sectional area to the selected angle, it is possible to reduce the amount of normal stresses in the cross-section. From the above dependences, as well as looking through the prism of previous material tests, it appears that the optimal angle of the cutting line should oscillate in the area of 60° to the longitudinal axis of the profile, however due to the different shape, and more precisely the width of the flat profiles from which the structure is built vehicle frame, this solution should be adopted so that, with the size of the side walls imposed by the dimensions of this profile, the optimal and consistent working width "X", the profile joining area, matched to the technical capabilities of such a process is maintained. However, the reduction of normal stresses is accompanied by an increase in tangential stresses, which were dealt with using a geometric solution.

6. Geometric solution to the problem

The reduction of normal stresses in the cross-section, in the repaired frame, by changing the angle of the cutting line and the associated weld connection, implies the appearance of tangential stresses. According to the theory of stress state, the greatest tangential stresses occur in cross-sections inclined to the main directions at an angle $\pi/4$ and amount to uniaxial stress state $\tau_{max}=Ϭ/2$. The solution to the problem of the occurrence of tangential stresses associated with the proposed change of the cutting line angle was sought in the method of guiding the section line so that the shape of the joint would use natural features partially

eliminating the problem. The geometrical solution allowing to meet the above assumption seemed to be the shape of a combination of two elements of a rectangular profile arranged with bends. This opposite configuration of two joined fragments uses its geometric properties in a natural way. On the one hand, taking into account the above concept, cuts at an angle, on the other hand, ending the danger of cutting such connected fragments through a geometric clinch, e.g. as a result of sudden stress caused, for example, by a vehicle collision. The diagram (Fig. 3.8) shows the proposed solution for symmetrical and asymmetrical sections.
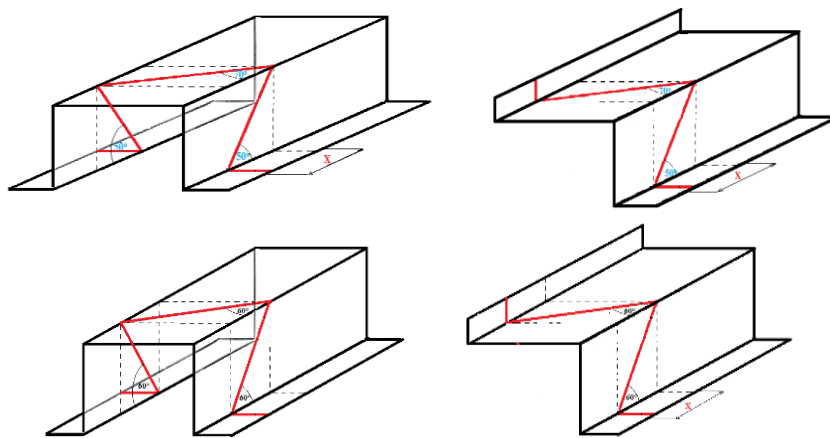

Fig. 3.8. Scheme of class I,II,III profiles, with cut/joining lines in the welding process, for exemplary sections with marked work area "X".

7. Modeling and numerical analysis of the structure of oneomega profile with the change of the cutting line angle.

Analogically to the previous simulations, this time calculations were made for the model on which two applications were applied. The first one referred to the conventional method and can be observed on the upper part of the hat model. Next, the geometry of the model was modified by changing the course of the connection, leading it at an angle of 60° to the cross-section. The introduction of an application to anticipate the conventional and alternative methods on one model was fully intentional, because only in this way was it possible to visualize the differences in concentration of stress in the areas of these applications for the proposed uniaxial state of stress using the following visualization and color.
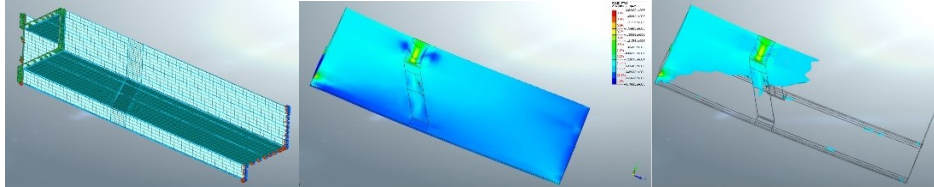
Fig. 3.9. The proposed geometric shape of the side-member and the application of the welded connection

8. Conclusion

If in the case of class I,II,III profiles the proposed solution seems satisfactory in the context of maintaining strength properties similar to the native material from which the construction was made, after the connection process, regardless of whether it is carried out at the pre- or post-production stage vehicle, it should be noted that these considerations apply only to profiles I,II,III, that is, where the Saint-Venanta principle applies. At the beginning of this article, it was emphasized that it is equally important to present limitations to the proposed method, so that this solution could be properly used and not exposed to depreciation. Therefore, it should be said that the above method is not suitable for class IV profiles (in which this principle is abolished). The results of model and experimental studies of class IV profiles have not been presented in this study because they go beyond the scope of this article. They clearly demonstrated that the strength properties of a welded joint that formed a bend influenced the weakening of its bearing properties in relation to the conventional method, clearly disqualifying this method for this class profiles [13].

References

[1] https://www.audanet.pl/,. http://datpolska.pl/home.html, programy komputerowe do kosztorysowania napraw pojazdów.
[2] Volkswagen GP, GBSA00, „Podstawy konstrukcji i napraw powypadkowych karoserii" wersja z dnia 13.03.2015.
[3] Hadryś D. (2009). Wpływ naprawy powypadkowej metodami spawalniczymi na bezpieczeństwo bierne konstrukcji nośnych pojazdów. Praca doktorska, Politechnika Śląska. Wydział Transportu. Katedra Eksploatacji Pojazdów Samochodowych.
[4] S. Krajewski, J. Nowacki (2014). Dual-phase steels microstructure and properties consideration based on artificial intelligence techniques, Archives of Civil and Mechanical Engineering (ISSN: 1644-9665, Tom: 14, Zeszyt: 2, Strony: 278-286)
[5] SSAB., Advanced High Strength Steels For Th e Automotive Industry, SSAB SE-781 84 Borlänge Sweden
[6] SSAB, Docol DP/DL Zimnowalcowana stal dwufazowa, SSAB EMEA AB SE-781 84 Borlänge Sweden

[7] Z. Gronostajski, R. Kuziak (2010), Metalurgiczne, technologiczne i funkcjonalne podstawy zaawansowanych wysokowytrzymałych stali dla przemysłu motoryzacyjnego. Prace IMŻ 1

[8] M. Nowicki, K. Ukasik, J. Tomczak, R. Czachor, J. Kuc (2014). Problematyka wytwarzania wyrobów ze stali AHSS, PM rok wyd. LXXIII ZESZYT 5/2014

[9] R. Molenda, R. Kuziak (2011). Metaloznawcze podstawy kształtowania struktury i właściwości blach ze stali DP w procesie ciągłego wyżarzania, Instytut Metalurgii Żelaza, Prace IMŻ 2

[10] A. Ambroziak, P. Białucki, W. Derlukiewicz, A. Lange (2014). Właściwości złączy spawanych ze stali dwufazowej DP600 metodą. MAG Agenda Wydawnicza SIMP. Przegląd Spawalnictwa. 9/2014.

[11] J. Senkara (2009). Współczesne stale karoseryjne dla przemysłu motoryzacyjnego i wytyczne technologiczne ich zgrzewania. Przegląd spawalnictwa. 11/2009.

[12] T. Węgrzyn, D. Hadryś, M. Miros (2008). Połączenia spawane wykonywane podczas napraw powypadkowych nadwozi pojazdów samochodowych. Przegląd spawalnictwa. 2/2008.

[13] (2018) Preliminary tests of post-repair properties of the vehicle body energy-consuming structures. International Automotive Conference (KONMOT2018), IOP Conf. Series: Materials Science and Engineering 421 032008, IOP Publishing, doi:10.1088/1757-899X/421/3/032008.

[14] R. Urtbanik. Ramy pojazdów samochodowych. ZSM Opole.

Chapter 4.

Joanna ZIELIŃSKA-SZWAJKA[1*]
Marek KOCHAN[1]

MACHINABILITY OF TI6AL4V TITANIUM ALLOY IN THE DRILLING PROCESS

Abstract
Titanium alloys are widely used in various industries and the economy (aeronautics, medicine, etc.). This is due to favorable properties such as: corrosion resistance, good mechanical strength and high relative strength coefficient. The article presents the analysis of selected machinability indexes of Ti6Al4V titanium alloy in the drilling process based on the measurement of cutting edge temperature (T), thrust force (F_f), cutting torque (M_z) and selected surface roughness indexes (Ra, Rz). The tests used a drill made of sintered carbide with a coating TiAlN. The temperature measurement was carried out using an industrial temperature track with a K type thermocouple. A piezoelectric sensor was used to measure the value of the thrust force and cutting torque. Roughness measurement was carried out on a stationary profilometer. On the basis of studies it was observed that the temperature in the drilling Ti6Al4V titanium alloy affect cutting speed (v_c) and the feed (f). A significant influence of the feed value on the value of thrust force, cutting torque and surface roughness of the machined surface was observed.

Keywords:
Ti6Al4V titanium alloy, drilling, temperature, thrust force, cutting torque, surface roughness.

1. Introduction

Titanium and its alloys are distinguished from other construction materials used primarily due to their high relative strength (Rm/δ) in a very large temperature range and very high corrosion resistance in many chemically aggressive environments.

---

[1] Faculty of Mechanics and Technology, Rzeszow University of Technology, Kwiatkowskiego 4, 37-450 Stalowa Wola, Poland;
* j.zielinska@prz.edu.pl

The strength of titanium alloys is also definitely higher than the relative strength of aluminum and magnesium alloys it increases with the working temperature, therefore they are very widely used in aviation. Titanium and its alloys are also widely used in the construction of chemical apparatus and machines due to the high corrosion resistance. Other titanium properties also include: high melting point, non-magnetic, biological inertness or even a small coefficient of thermal expansion. The remarkable properties of titanium alloys allow significant opportunities to improve technological processes, tooling and manufacture of products in the most various branches of the economy and industry [1, 2].

Titanium alloys are increasingly used with other metals such as aluminum, iron, tin, vanadium, molybdenum, etc. These alloys are characterized by high Rm strength, relative elongation and low thermal conductivity. The last of these characteristics of these alloys make them very difficult to machine alloys. High plasticity and strength contribute to the formation of a large amount of heat in the cutting process, which at a relatively low thermal conductivity is dissipated to a large extent by the blade, and to a minimum by the chip produced in the cutting process. It is recommended to use an abundant supply of cooling lubricants. At low cutting speeds, oil liquids are desirable, while at higher cutting speeds, emulsion fluids.

Cutting forces have values definitely lower than in the case of steel machining and the pressure near the edge is greater, which, together with the increased temperature, results in a significantly shorter blade life. Pure titanium as a material does not affect the build-up, but there is a tendency to stick chips to the tool, which is very undesirable when using interrupted cuts. For machining titanium and its alloys, fine-grained tungsten carbides, uncoated (as for cast iron) are used, because titanium rapidly diffuses from the tool to the chip. The use of Al ceramics also affects rapid wear of the blade by abrasion [4].

Titanium is included in the material group S, together with heat-resistant super alloys. Titanium and its alloys as construction materials have a very low thermal conductivity. As the temperature increases, the rate of thermal conductivity of titanium decreases. Alloy additives change the thermal conductivity of titanium. In the case of Ti6Al4V titanium alloy, the addition of aluminum significantly reduces thermal conductivity at low temperature. It should be emphasized that the effect of temperature on the thermal conductivity in titanium alloys depends particularly on the aluminum content. Additionally, small amounts of vanadium increase the thermal conductivity of alloys [2].

Nowadays, titanium and its alloys are widely used in all areas of life and industries. The special properties of these construction materials are the merit of this. The basic and one of the most common titanium alloys, which is characterized by very good plasticity and strength is Ti6Al4V titanium alloy.

Due to the fact that titanium is a very expensive material and has special properties compared to other construction materials, its use is specific depending on the field [2]. Titanium as an element and its alloys are widely used in various areas of life, including aviation, machine, food, chemical, medicine and shipbuilding industries. The unique use of titanium and its alloys results from the fact that it achieves the highest ratio of mechanical strength to density and high corrosion resistance [5].

In machine building and processing plants, machining is the basic method of forming, accounting for about 70% of all object shaping techniques. Drilling is one of the most frequently performed operations during machining processes. The drilling process can be done on a pre-made or pre-cut basis, leaving allowance for further processing. Material separation in the drilling process is much more difficult than when turning. At the initial stage of drilling, the cutting edge is indented in the workpiece, causing its plastic deformation, until the material is separated by the main cutting edge. The auxiliary cutting edge is intended to smooth the hole surface. The processes of chip evacuation and supply of cooling lubricants to the machining space during drilling are very difficult, as a result of which a significant amount of heat penetrates the cutting tool causing its accelerated wear. Shaping operations by drilling are most often performed on drills and milling machines and on lathes when the hole being made is in the axis of rotation of the workpiece.

Temperature and heat play an essential role in cutting processes, significantly affecting the intensity of blade wear and shaping the surface layer of the workpiece. During the cutting process efficient operation is converted into heat.

There are many methods for measuring blade temperature. They are more or less complicated [3]. Thermoelectric methods are the most common methods for measuring the cutting temperature. Among other methods, photoelectric methods deserve more attention, which rely on the heat radiation of the body under examination. Thermoelectric methods for measuring the cutting temperature are also called contact or contact methods, due to the heat conduction between the sensor and the test body, they rely on the use of various physical phenomena that are indirectly associated with the thermocouple. Contact methods are divided into non-electric and electrical. In the case of measurements with non-electric devices, they use the phenomenon of thermal expansion of solids, liquids and gases.

Electric instruments for measuring temperature in the cutting process can be divided depending on the physical phenomenon used into semiconductor, resistance and thermoelectric. The disadvantage of photoelectric methods is the low measuring accuracy, resulting primarily from the difficulty of calibrating instruments and obtaining constant characteristics of the radiating surface during cutting. Calorimetric methods are used in the heat balance measurements.

2. Research methodology
2.1. Workpiece and cutting tool

The processed material used in the study was Ti6Al4V titanium alloy. The chemical composition of the titanium alloy used in the study was determined on the basis of spectral analysis by means of the MIRA3 scanning electron microscope with the TESCAN EDS attachment (Fig. 4.1), which is shown in Fig. 4.2.

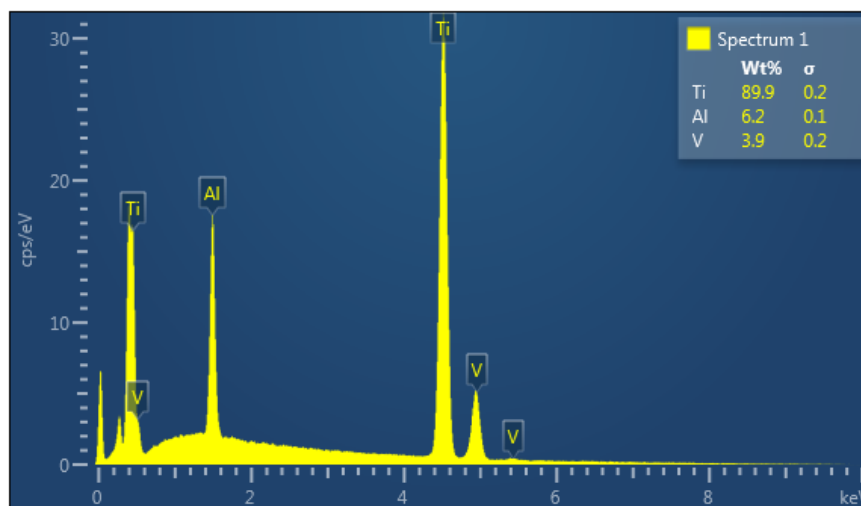Fig. 4.1. Scanning electron microscope with TESCAN EDS attachment

Fig. 4.2. Results of spectral analysis of the Ti6Al4V

Fig. 4.3. Microphotograph of an Ti6Al4V panel surface

In the tests carried out, a ISCAR through hole drill (SDC 061-043-080 ACP5N) with a diameter of ø 6.1 mm with cemented carbide blades, TiAlN-coated was used as a cutting tool. This tool belongs to two-edge drills, it is primarily used for machining titanium alloys in industrial conditions on numerically controlled machine tools. The photo of the drill used for the tests carried out in the titanium alloy Ti6Al4V with geometric parameters is shown in Fig. 4.4.
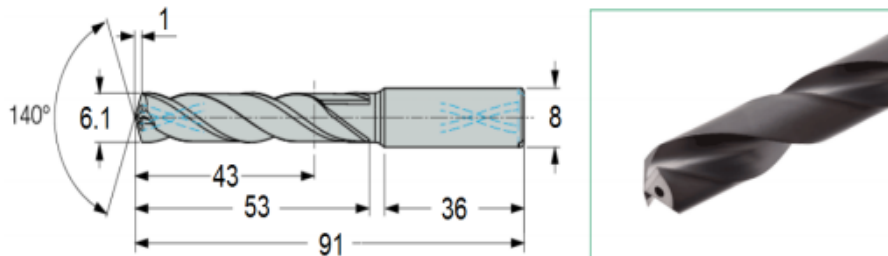
Fig. 4.4. Cutting tool used in the research

2.2. Measurement of cutting forces

As part of the tests, axial force and cutting moment were measured during drilling. To measure these values, a 2-component piezoelectric force and cutting moment sensor from KISTLER type 9345B2 was used together with the load preamplifier type 5073A211 (Fig. 4.5).

Fig. 4.5. Axial force (F_f) and cutting moment (M_z) sensor type 9345B2 with 5073A211 charge preamplifier

The tests were carried out on an EMCO vertical milling machine with an installed system for measuring cutting forces (Fig. 4.6).
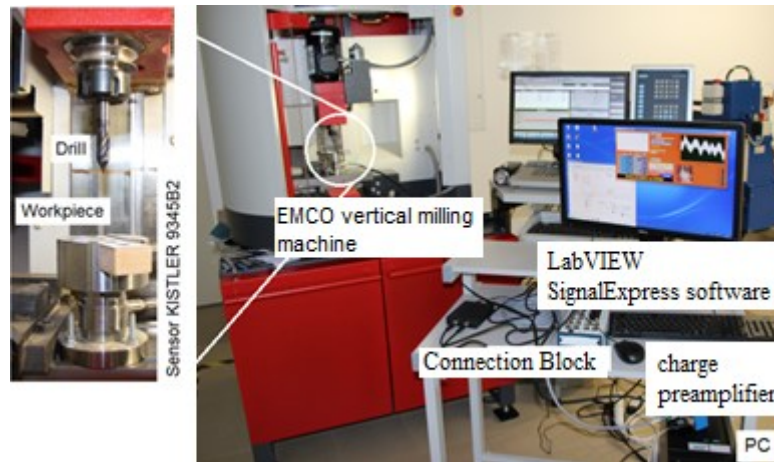
Fig. 4.6. Experimental set-up

The results of the tests were recorded by the LabVIEW SignalExpress software and saved on a PC for further analysis. The forces and cutting moments signals were sent to the NI PCI-6034E analog-to-digital converter card via the 5073A211 charge preamplifier. The measuring track used to measure the axial force and cutting moment is shown in Fig. 4.7.

Fig. 4.7. Schematic diagram of the data acquisition system

Drilling tests were carried out without the use of a cooling lubricant, thus facilitating the observation of the cutting zone and the process of chip formation. It was decided to drill holes in a flat titanium alloy with dimensions $130 \times 22 \times 12$ mm for three values of cutting speed vc. For each of these speeds, tests were carried out for three values of feed f, as shown in Table 4.1.

Table 4.1. Parameters used in the studies

Cutting speed v_c m/min	Feed f mm/rev.	Feed speed v_f mm/min
10	0.05	26.25
10	0.10	52.50
10	0.15	78.75
20	0.05	52.25
20	0.10	104.50
20	0.15	156.75
30	0.05	78.50
30	0.10	157.00
30	0.15	235.50

2.3. Temperature measurement

Within the scope of the tests, temperature measurements were made during the drilling process. The temperature was measured during drilling on an EMCO lathe with an installed measuring track (Fig. 4.8). The temperature was measured using a K-type thermocouple.
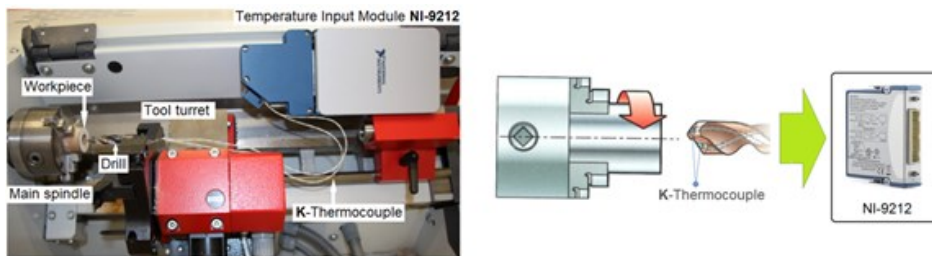
Fig. 4.8. Test stand and measuring track

The temperature was measured for three cutting speeds v_c m/min. Each of the individual cutting speed values was assigned three feed values f mm/rev. as shown in Table 4.1.

2.4. Roughness measurement

The surface roughness measurement was performed using the Hommel-Etamic T8000RC stationary profilometer (Fig. 4.9).
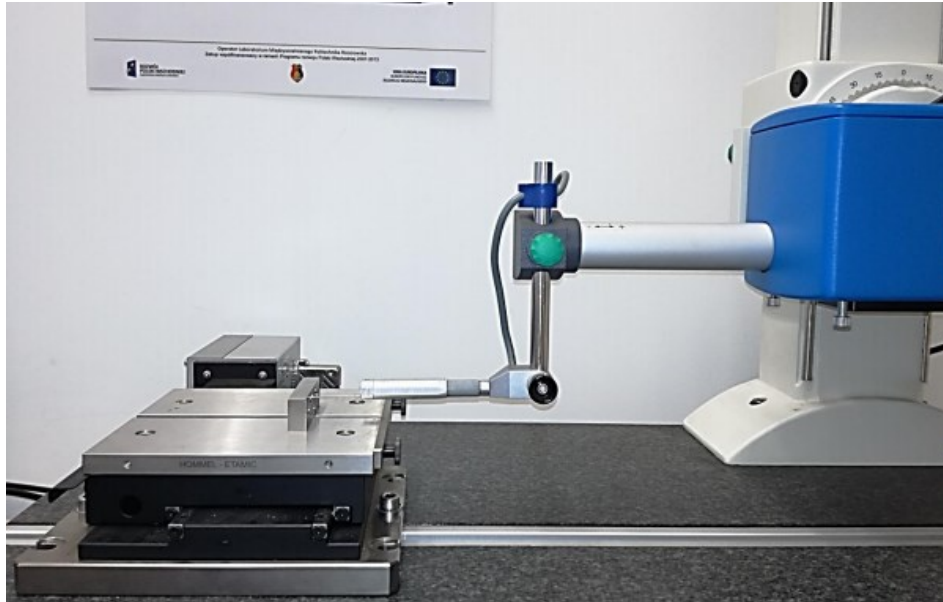
Fig. 4.9. Measurement of surface topography

The device allows the measurement of roughness (R), primary profile (P) and wave (W) parameters in accordance with ISO, DIN and JIS standards. It is also possible to perform measurements and tests of the surface layer roughness parameters in a 3D system, i.e. in the geometric structure of the SGP surface.

3. Test results
3.1. Measurement of cutting forces
Figure 4.10 illustrates the variations in feed force and cutting moment as a function of drilling depth when drilling Ti6Al4V titanium alloy.
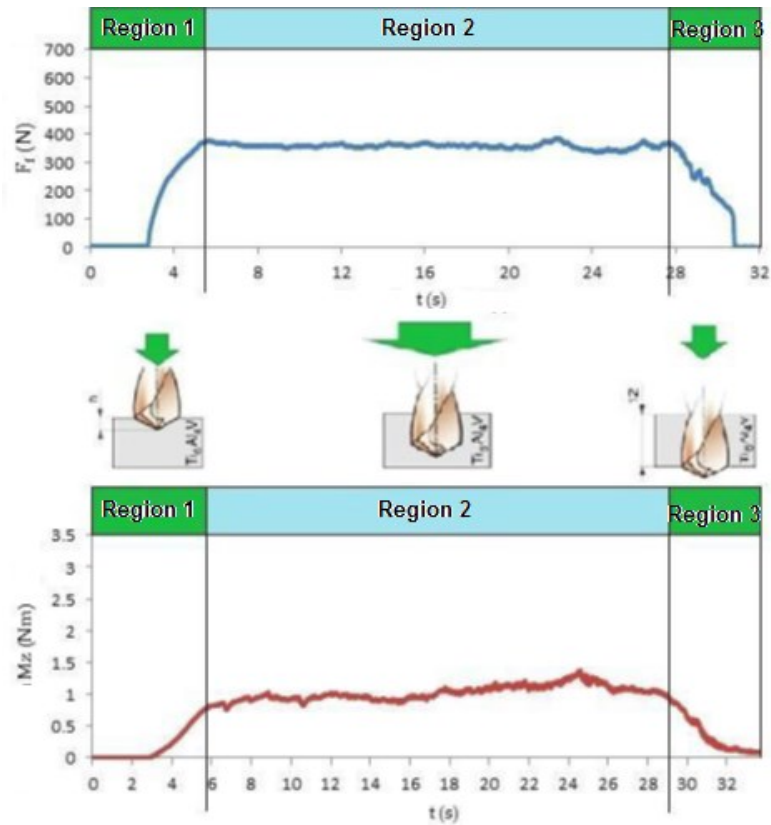
Fig. 4.10. Variation of axial force (F_f) and cutting moment (M_z) in the drilling process

After the measurements are taken, three main areas can be observed during the analysis of the tests, which affect the characteristics of the change in the value of the axial force F_f and the cutting moment M_z. In the first area presented, the value of the axial force increases very quickly, reaching a maximum value of over 600 N for a cutting speed of $v_c = 10$ m/min and a feed value of $f = 0.15$ mm/rev. The increase in the axial force is caused by the drill sinking into the workpiece. The first area is assumed for a drill whose cutting path h is equal to the value of the height of the cutting edges of the tool. The value of h = 1 mm was used for the tests. In the second area, the phenomenon of axial force stabilization can be observed, this is due to the entry of the cutting tool blade into the deeper drilling area of the titanium alloy. After the tests, it is also found that the oscillations of the diagrams in the presented second area may be caused by a local change in the microstructure properties of the tested construction material, as well as the occurrence of local harder zones in the material. The transition of the diagrams

60

to the third area allows to state that the drill reaches the final stage of making the through hole where it finally goes beyond the area of the drilled material, which is associated with a sharp decrease in the value of the axial force, which decreases to zero when withdrawing the drill from the hole. Changes in cutting time t s with respect to the material being tested are due to the increase in the feed rate v_f mm/min as well as the cutting speed v_c m/min. Regarding the cutting moment, we deal with the same areas that occurred in the case of the axial force tested. The position of the drill depth relative to the tested sample allows to determine how the value of the cutting moment is distributed during the drilling process. The highest cutting torque value of 3.4 Nm is recorded for the test in which the technological parameters were set as follows: cutting speed v_c = 30 m/min and feed speed v_f = 235.5 mm/min. A minimal increase in the cutting moment value during the final drilling phase may be related to chip retention in the machining area or resulting vibration.
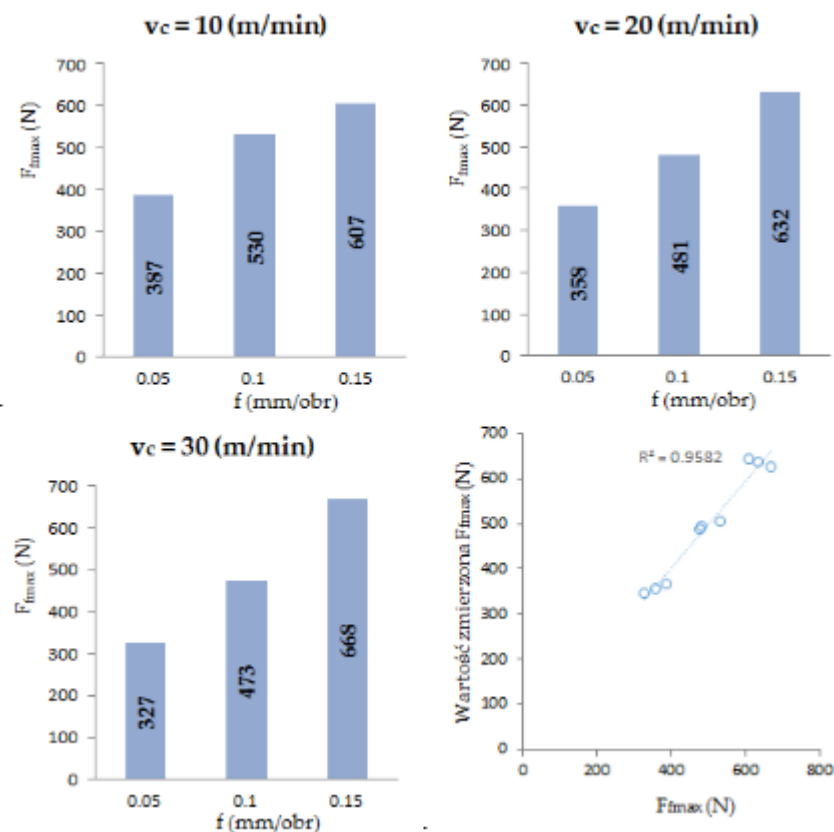

Fig. 4.11. Influence of the feed value on the value of the axial force

Figure 4.11 shows the dependence of the axial force (F_f) on the feed value for three cutting speeds.

The value of the axial force can be described by the relationship:

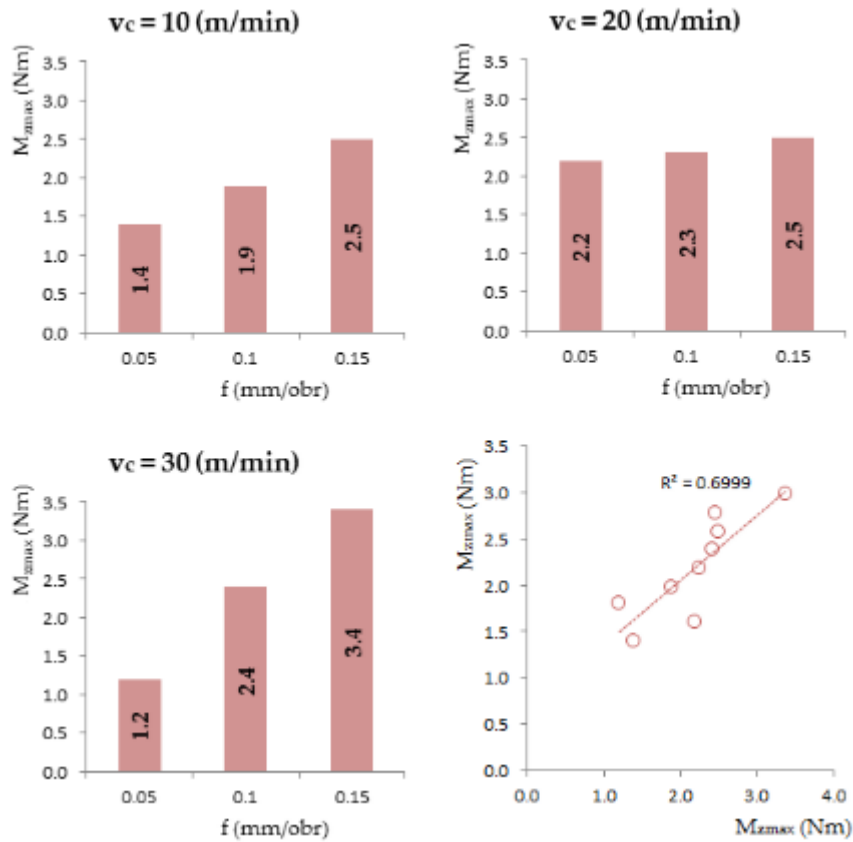$$F_f = 235.77 - 0.93 \cdot v_c + 2785.67 \cdot f \tag{1}$$

Fig. 4.12. Influence of the feed value on the value of the cutting moment

Figure 4.12 shows the dependence of the cutting moment (M_{zmax}) on the feed value for three cutting speeds.

The value of the axial force can be described by the relationship:

$$M_z = 0.59 + 0.02 \cdot v_c + 11.8 \cdot f \tag{2}$$

3.2. Temperature measurement

Research on temperature measurement in the titanium alloy drilling process was performed for the same parameters as for cutting resistance. The maximum temperature value recorded during the measurements was T = 452 °C for a cutting speed of v_c = 30 m/min and a feed value of f = 0.05 mm/rev. The Ti6Al4V titanium alloy as a construction material belongs to the group that is characterized by very high temperatures that can be noted when conducting tests of this type of alloys. It can be stated that the temperature value in the tests depends, among others on the cutting speed value and the feed value, on which the drilling time t (s) also depended. In the measurements carried out, the temperature value was comparable for the cutting speed of v_c = 20 m/min. It can also be stated that in the case of the measurement for cutting speed v_c = 20 m/min and feed value f = 0.05 mm/rev, the temperature value is much higher compared to the measurement with the cutting speed value v_c = 10 m/min using the same value feed rate f.

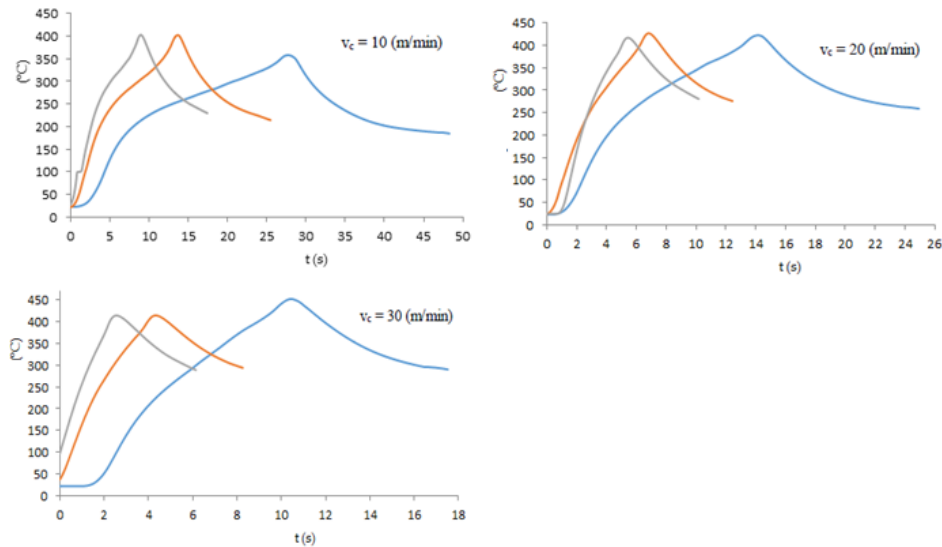The relationship between temperature and cutting parameters is shown in Figure 4.13.

Fig. 4.13. T °C signal waveforms depending on parameters
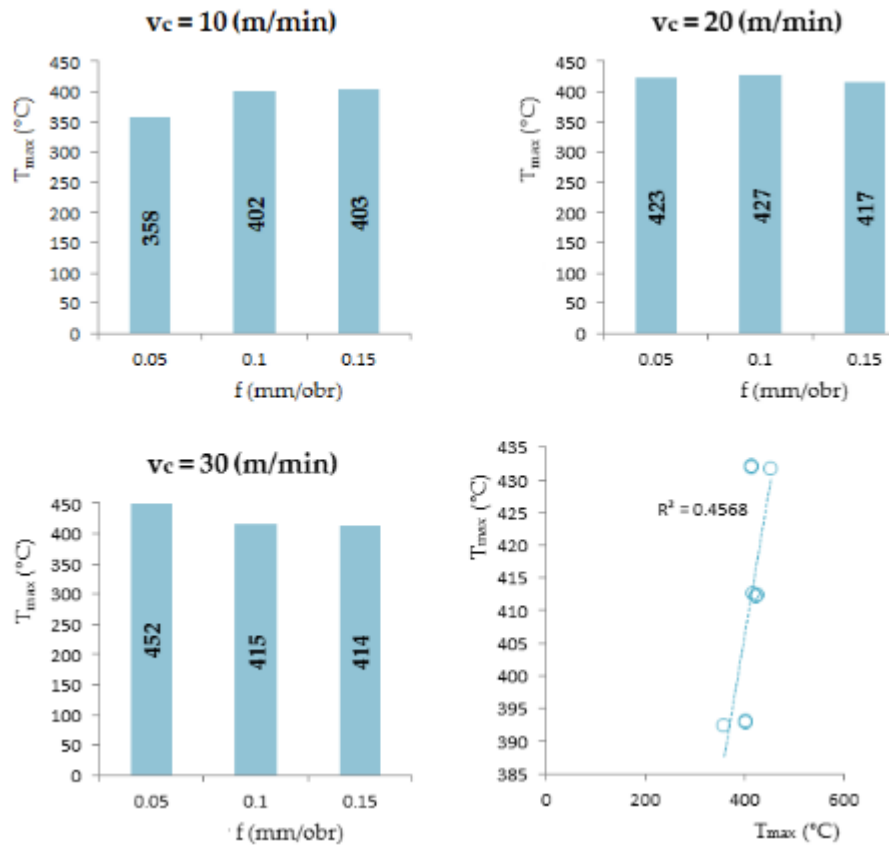
Fig. 4.14. Influence of the feed value on the value of the temperatures

Figure 4.14 shows the dependence of the cutting moment (T_{max}) on the feed value for three cutting speeds.

The maximum temperature value can be described by the relationship:

$$T = 372.54 + 1.97 \cdot v_c + 5 \cdot f \tag{3}$$

3.3. Roughness measurement

Studies regarding the measurement of roughness in the drilling process of titanium alloy have been carried out for the same parameters as for cutting resistance and temperature. For the assumed values of technological parameters, roughness measurements were made in 10 tests in order to determine the average and maximum values.

The length of the measuring section for each test was L = 4.8 mm. For individual tests of surface roughness measurements, roughness profile charts were prepared, as well as detailed maps of the topography of the tested surfaces in 3D views.
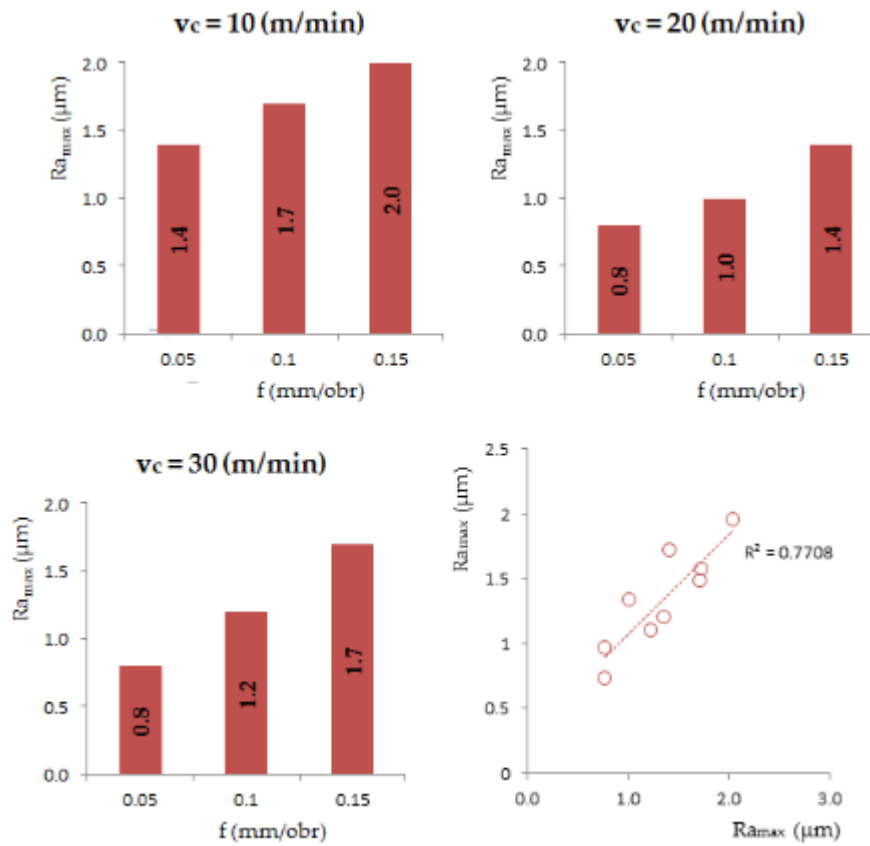

Fig. 4.15. Influence of the feed value on the value of the Ra

The Ra value can be described by the relationship:
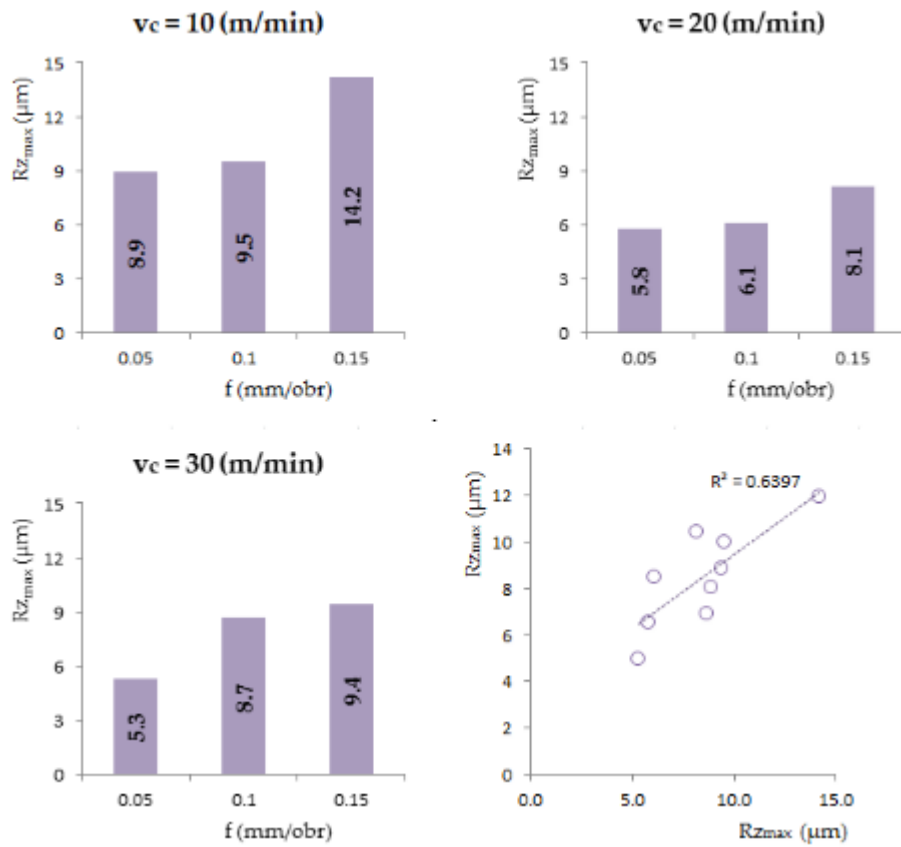
$$Ra = 1.06 - 0.02 \cdot v_c + 7.57 \cdot f \tag{4}$$

Fig. 4.16. Influence of the feed value on the value of the Rz

The Rz value can be described by the relationship:

$$Rz = 7.63 - 0.154 \cdot v_c + 39.03 \cdot f \tag{5}$$
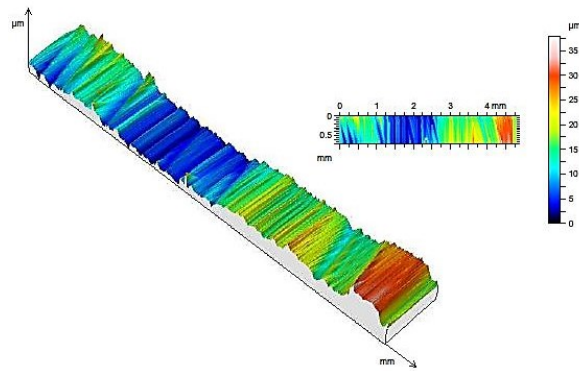
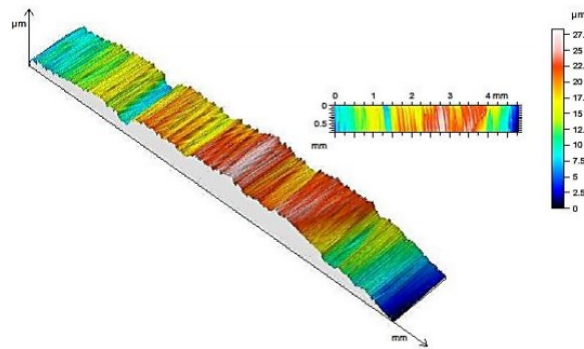Fig. 4.17. Topography of the hole surface for vc = 10 m/min, f = 0.15 mm/rev.

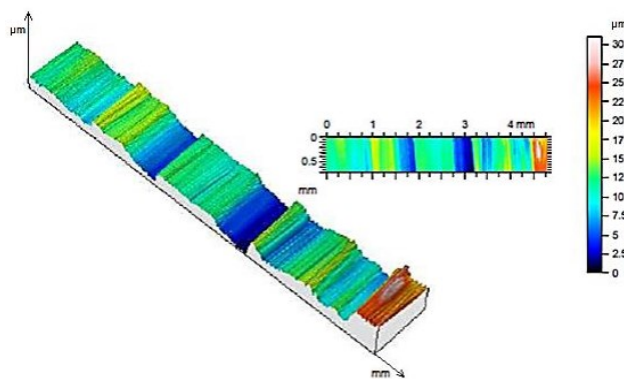Fig. 4.18. Topography of the hole surface for vc = 20 m/min, f = 0.15 mm/rev.

Fig. 4.19. Topography of the hole surface for vc = 20 m/min, f = 0.15 mm/rev.

Figs. 4.17 – 4.19 show sample surface topographies at constant feedrate f = 0.15 mm/rev and variable cutting speed values v_c = 10 ÷ 30 m/min. Based on topographic maps and test results, it was found that for the tests performed, the worst hole quality was obtained with the cutting speed value of v_c = 10 m/min. The lowest averaged Ra of 0.70 μm was obtained for the cutting speed of v_c = 30 m/min and the feedrate of f = 0.05 mm/rev., maximum 1.77 (μm) for the cutting speed of v_c = 10 m/min and feed values. During the analysis of the conducted tests it was found that in the case of the cutting speed value of v_c = 10 m/min with the increase of the feed value f mm, the average and maxi-mum values Ra and Rz increase. The maximum value of the roughness height was Rz_{max} = 14.2 μm. In the case of cutting speed v_c = 20 m/min and feed speed values f = 0.10 mm/rev, the average surface roughness was Ra = 0.98 μm, while for cutting speed v_c = 30 (m / min) and feed values f = 0.05 mm/rev the mean surface roughness value was Ra = 0.70 μm.

4. Conclusions

After analyzing the test can be made the following conclusions:
- A significant influence of feed values on the value of thrust force as well as the torque moment was observed. An increase in the feed value results in an increase in the value of the thrust force and the torque moment;
- The temperature in the process of drilling Ti6Al4V titanium alloy depends on the cutting speed. The feed speed has no significant effect on the temperature.;
- The feed rate has a significant influence on the roughness of the machined surface. As the feed rate increases, the analyzed roughness indexes increase.

References

[1] Błaszczuk W., Melechow R., Tubielewicz K. (2004). *Tytan i jego stopy. Gatunki. Właściwości. Zastosowanie. Technologia obróbki. Degradacja*. Wydawnictwo Politechniki Częstochowskiej, Częstochowa.
[2] Bylica A., Sieniawski J. (1985). *Tytan i jego stopy.* Springfield, IL: Państwowe Wydawnictwo Naukowe, Warszawa.
[3] Jemielniak K.. (2018). *Obróbka skrawaniem*. Oficyna Wydawnicza Politechniki Warszawskiej, Warszawa.

[4] Szwajka K., Zielińska-Szwajka J., Trzepiecinski T. (2019). *Experimental Study on Drilling MDF with Tools Coated with TiAlN and ZrN*. (12)386: [s. 4-7]

[5] (1995). *Tytan i jego stopy: przetwórstwo i zastosowanie w technice*. materiały IV Ogólnopolskiego Sympozjum. Oficyna Wydawnicza Politechniki Rzeszowskiej, Rzeszów – Łańcut [s. 88, s. 126]

Streszczenie

MATERIAL, TECHNOLOGIES, CONSTRUCTIONS: "Special purpose technologies" to monografia składająca się z czterech rozdziałów o tematyce dotyczącej technologii specjalnego przeznaczenia. W rozdziale pierwszym poruszono zagadnienia dotyczące technologii spawania stali ARMOX. W rozdziale przedstawiono badania właściwości makro i mikrostruktury oraz twardości obszaru złączy spawanych wykonanych. Analizowano złącza doczołowe, pachwinowe oraz narożne. Tematyka spawania stali ARMOX jest bardzo ważnym zagadnieniem w przemyśle maszyn budowlanych oraz zbrojeniowym. Rozdział drugi dotyczy zagadnień mechanizmu zderzenia cząstek proszku metalicznego podczas natryskiwania termicznego stali. W pracy analizowano mechanizm rozpryskiwania się kropli ciekłego metalu podczas zderzenia z powierzchnia natryskiwaną. Określono strukturę geometryczną powierzchni, wykonano badania metalograficzne oraz opisano mechanizm zderzeń. Tematyka ta jest istotna dla projektowania procesów natryskiwania termicznego w celu zwiększenia odporności mechanicznej lub termicznej powierzchni elementów współpracujących w konstrukcjach maszyn i urządzeń. Rozdział trzeci dotyczy tematyki związanej z technologią naprawy ram nośnych samochodów ciężarowych. Prezentowana technologia dotyczy procesu spawania. Określono właściwości mechaniczne twardość, wytrzymałość oraz naprężenia. Czwarty rozdział porusza zagadnienia z zakresu obróbki skrawaniem stopu tytanu. Podczas badań wykonywano pomiary zmian temperatury podczas obróbki. Przeprowadzono obserwacje metalograficzne, określano strukturę geometryczną powierzchni stopu po obróbce.

Abstract

MATERIAL, TECHNOLOGIES, CONSTRUCTIONS: "Special purpose technologies" is a monograph consisting of four chapters on special purpose technologies. The first chapter deals with ARMOX steel welding technology. The chapter presents the investigations of macro- and microstructure properties and hardness of the area of performed welded joints. Frontal, fillet and corner joints were analysed. The topic of welding of ARMOX steels is a very important issue in the construction and armaments machinery industry. The second chapter deals with the mechanism of collision of metallic powder particles during thermal spraying of the steel. The paper analyses the mechanism of spattering liquid metal droplets during the collision with the sprayed surface. The geometric structure of the surface was determined, metallographic tests were performed and the mechanism of collisions was described. This subject matter is important for the design of thermal spraying processes in order to increase the mechanical or thermal resistance of the surface of cooperating elements in the construction of machines and devices. The third chapter concerns the issues related to the technology of repair of trucks frame bearers. The technology presented here concerns the welding process. Mechanical properties of hardness, strength and stress were determined. The fourth chapter deals with the issues of the machining of titanium alloy. During the tests, temperature changes during machining were measured. Metallographic observations were carried out and the geometric structure of the surface of the alloy after machining was determined.